Available online at www.sciencedirect.com
SCIENCE DIRECT®
Physica D 211 (2005) 347–376
PHYSICA D
www.elsevier.com/locate/physd

Heteroclinic cycles and periodic orbits for the O(2)-equivariant 0:1:2 mode interaction

T.R. Smith[a,*], J. Moehlis[b,1], P. Holmes[a,b]

[a] *Department of Mechanical and Aerospace Engineering, Princeton University, Princeton, NJ 08544-5263, USA*
[b] *Program in Applied and Computational Mathematics, Princeton University, Princeton, NJ 08544-1000, USA*

Received 27 January 2005; received in revised form 12 August 2005; accepted 7 September 2005
Communicated by A. Doelman
Available online 3 October 2005

Abstract

We study the quadratic normal form describing the generic interaction of Fourier modes of wavenumbers 0, 1 and 2 under the symmetry group O(2) of rotations and reflections, in the case that the homogeneous quadratic terms preserve 'energy': the sum of the squares of absolute values of the (complex) variables. This system is a generalization of the 1:2 mode interaction studied by Dangelmayr [G. Dangelmayr, Steady-state mode interactions in the presence of O(2)-symmetry, Dyn. Stab. Syst. 1 (2) (1986) 159–185], Armbruster et al. [D. Armbruster, J. Guckenheimer, P. Holmes, Heteroclinic cycles and modulated travelling waves in systems with O(2) symmetry, Physica D 29 (1988) 257–282] and others, and its restriction to the 1:2 subspace is a degenerate case of that system. It displays all the classes of fixed points, periodic orbits (standing and travelling waves), invariant tori (modulated travelling waves) and heteroclinic cycles found in the 1:2 interaction, as well as new heteroclinic cycles connecting pure and mixed modes, chaotic cycles, and 'strange' periodic orbits. We describe the key dynamical features, show that the degenerate 1:2 case possesses a second organizing center at which bifurcation curves coalesce, provide representative bifurcation sets and diagrams for the 1:2 and 0:1:2 systems, and use a conservative limit to understand the periodic orbits in the latter system.

Keywords: Mode interactions; Bifurcations; Heteroclinic cycles

1. Introduction

In this paper we consider the normal form, truncated at quadratic order, for the 0:1:2 spatial resonance in the presence of O(2) symmetry near a codimension three bifurcation point. The state variables a_j, $j = 0, 1, 2$ represent

* Corresponding author. Present address: Control and Dynamical Systems, California Institute of Technology, Mail Stop 107-81, 1200 E. California Blvd, Pasadena, CA 91125, USA. Tel.: +1 626 372 9024; fax: +1 626 796 8914.
[1] Department of Mechanical and Environmental Engineering, University of California, Santa Barbara, CA 93106, USA.
E-mail address: trsmith@cds.caltech.edu (T.R. Smith).

0167-2789/$ – see front matter © 2005 Elsevier B.V. All rights reserved.
doi:10.1016/j.physd.2005.09.002

the amplitudes of Fourier modes having wavenumbers 0, k and $2k$; thus, assuming a real physical field, $a_{1,2}$ are complex variables and a_0 is real. We further restrict our study to the special, but physically important, case in which the homogeneous quadratic terms preserve a norm corresponding, for example, to kinetic energy of a fluid. Indeed, the following system arose in our studies of low-dimensional models of plane Couette flow [3,4], and this provided our initial motivation. This three-way interaction also appears to play an important role in another recent fluid study, of counter-rotating swirling flow, which has bifurcation behavior which cannot be fully explained by the 1:2 resonance [5].

The 0:1:2 system at once generalizes, and, in a limiting form, represents a special degenerate case of, the 1:2 spatial resonance studied by Dangelmayr [1] and Armbruster et al. [2], hereafter referred to as AGH. This system, which was simultaneously and independently investigated by Jones and Proctor [6,7], provided the first analytically-tractable example of structurally stable heteroclinic cycles, which had also been identified slightly earlier in a model of the boundary layer [8]. Such cycles were subsequently found in numerous fluid and other contexts: for a particularly clear recent example, see Mercader et al. [9].

Structurally stable heteroclinic cycles and the periodic and quasiperiodic orbits that are associated with them are physically important since they provide a robust mechanism by which unstable transients can repeatedly occur in dynamical problems. In turbulent and preturbulent fluid flows the parts of these cycles near saddle points correspond to coherent structures: organized vortical and shear layer structures that appear, evolve, disappear and reappear cyclically but not generally periodically [10]. Also see the introductory remarks in Sections 4 and 5.

In this paper we show how the bifurcation sets of the 0:1:2 and the 1:2 resonances are related, and describe phenomena not present in the 1:2 case, including 'multi-heteroclinic' cycles and strange periodic orbits. The equations for the 0:1:2 resonance may be written in the form:

$$\begin{aligned}\dot{a}_0 &= \mu_0 a_0 + 2(B_1|a_1|^2 + B_2|a_2|^2),\\ \dot{a}_1 &= (\mu_1 - B_1 a_0)a_1 + c a_1^* a_2,\\ \dot{a}_2 &= (\mu_2 - B_2 a_0)a_2 - c a_1^2,\end{aligned} \tag{1}$$

where $a_0 \in \mathbb{R}$ and $a_{1,2} \in \mathbb{C}$ and the parameters μ_j, B_j, c are real. For finite μ_0, we may remove c and μ_0 by rescaling the system via $t \mapsto |\mu_0|t$, $a_{0,1,2} \mapsto (c/|\mu_0|)a_{0,1,2}$, $\mu_{1,2} \mapsto \mu_{1,2}/|\mu_0|$, $B_{1,2} \mapsto B_{1,2}/c$ to arrive at the simpler form:

$$\begin{aligned}\dot{a}_0 &= \sigma_\mu a_0 + 2(B_1|a_1|^2 + B_2|a_2|^2),\\ \dot{a}_1 &= (\mu_1 - B_1 a_0)a_1 + a_1^* a_2,\\ \dot{a}_2 &= (\mu_2 - B_2 a_0)a_2 - a_1^2,\end{aligned} \tag{2}$$

where $\sigma_\mu \stackrel{\text{def}}{=} \text{sign}(\mu_0) = \pm 1$. We note that the parameter-rescaling symmetry $(a_j, \mu_j, t) \mapsto (\alpha a_j, \alpha\mu_j, t/\alpha)$ leaves (1) invariant, and thus it is only $B_{1,2}$ and the *ratios* $\mu_{1,2}/|\mu_0|$ that determine the system's qualitative behavior. In Section 6 we shall relax the assumption of nonzero μ_0 and we shall use the fact, noted above, that for $\mu_j = 0$, (1) preserves the 'energy' norm

$$E = \frac{a_0^2}{2} + |a_1|^2 + |a_2|^2. \tag{3}$$

We treat $\mu_{1,2}$ as bifurcation parameters (with $\mu \stackrel{\text{def}}{=} (\mu_1, \mu_2)$ denoting points in parameter space) and $B_{1,2}$ as system parameters. Allowing time reversal, we need only consider the two 'system cases' $B_{1,2} > 0$ and $B_2 < 0 < B_1$. It is noteworthy that both cases occur in low-dimensional models of plane Couette flow, the former in a moderate aspect ratio domain [3] and the latter in the minimal flow unit [4], the smallest domain able to sustain turbulence. We shall adopt parameter values derived in these papers for illustrative computations below.

The 0:1:2 resonance is related to a special case of the 1:2 resonance:

$$\begin{aligned}\dot{a}_1 &= a_1^* a_2 + (\mu_1 + e_{11}|a_1|^2 + e_{12}|a_2|^2)a_1,\\ \dot{a}_2 &= -a_1^2 + (\mu_2 + e_{21}|a_1|^2 + e_{22}|a_2|^2)a_2,\end{aligned} \tag{4}$$

studied in AGH [2], cf. [6,7,11] and references therein. The systems (2) and (4) will be compared in subsequent sections of this paper, in the course of which we shall use the real Cartesian and polar forms of (2):

$$\begin{aligned}\dot{a}_0 &= \sigma_\mu a_0 + 2(B_1 r_1^2 + B_2 r_2^2),\\ \dot{x}_1 &= (\mu_1 - B_1 a_0)x_1 + (x_1 x_2 + y_1 y_2),\\ \dot{y}_1 &= (\mu_1 - B_1 a_0)y_1 + (x_1 y_2 - y_1 x_2),\\ \dot{x}_2 &= (\mu_2 - B_2 a_0)x_2 - (x_1^2 - y_1^2),\\ \dot{y}_2 &= (\mu_2 - B_2 a_0)y_2 - 2x_1 y_1,\end{aligned} \tag{5}$$

$$\begin{aligned}\dot{a}_0 &= \sigma_\mu a_0 + 2B_1 r_1^2 + 2B_2 r_2^2,\\ \dot{r}_1 &= (\mu_1 - B_1 a_0)r_1 + r_1 r_2 \cos\,\phi,\\ \dot{r}_2 &= (\mu_2 - B_2 a_0)r_2 - r_1^2 \cos\,\phi,\\ \dot{\phi} &= \left(\frac{r_1^2}{r_2} - 2r_2\right)\sin\,\phi,\end{aligned} \tag{6}$$

where, with $r_{1,2}$ and $\theta_{1,2}$ defined to be non-negative moduli and real phase angles, respectively, $a_{1,2} \stackrel{\text{def}}{=} r_{1,2}\exp(\mathrm{i}\,\theta_{1,2}) \stackrel{\text{def}}{=} x_{1,2} + y_{1,2}\,\mathrm{i}$ for $\mathrm{i} \stackrel{\text{def}}{=} \sqrt{-1}$ and $\phi \stackrel{\text{def}}{=} 2\theta_1 - \theta_2$. As in [2], the emergence of the phase difference ϕ and reduction to four (real) dimensions is a consequence of O(2) equivariance. The analogous component forms of (4) are

$$\begin{aligned}\dot{x}_1 &= x_1 x_2 + y_1 y_2 + x_1(\mu_1 + e_{11}r_1^2 + e_{12}r_2^2),\\ \dot{y}_1 &= x_1 y_2 - y_1 x_2 + y_1(\mu_1 + e_{11}r_1^2 + e_{12}r_2^2),\\ \dot{x}_2 &= -(x_1^2 - y_1^2) + x_2(\mu_2 + e_{21}r_1^2 + e_{22}r_2^2),\\ \dot{y}_2 &= -2x_1 y_1 + y_2(\mu_2 + e_{21}r_1^2 + e_{22}r_2^2),\end{aligned} \tag{7}$$

$$\begin{aligned}\dot{r}_1 &= r_1 r_2\,\cos\,\phi + r_1(\mu_1 + e_{11}r_1^2 + e_{12}r_2^2),\\ \dot{r}_2 &= -r_1^2\,\cos\,\phi + r_2(\mu_2 + e_{21}r_1^2 + e_{22}r_2^2),\\ \dot{\phi} &= \left(\frac{r_1^2}{r_2} - 2r_2\right)\sin\,\phi.\end{aligned} \tag{8}$$

To demonstrate a connection between (2) and (4) we may employ the scaling $a_0 = \epsilon^2 s_0$, $r_{1,2} = \epsilon s_{1,2}$, $\mu_{1,2} = \epsilon^2 \nu_{1,2}$ and $\dot{(\,)} = \epsilon(\,)'$ to transform (6) to

$$\begin{aligned}\epsilon s_0' &= \sigma_\mu s_0 + 2(B_1 s_1^2 + B_2 s_2^2),\\ s_1' &= \epsilon(\nu_1 - B_1 s_0)s_1 + s_1 s_2\,\cos\,\phi,\\ s_2' &= \epsilon(\nu_2 - B_2 s_0)s_2 - s_1^2\,\cos\,\phi,\\ \phi' &= (\frac{r_1^2}{r_2} - 2r_2)\sin\,\phi;\end{aligned} \tag{9}$$

hence in the limit $\epsilon \to 0$ we may use the relation

$$s_0 = -2\sigma_\mu(B_1 s_1^2 + B_2 s_2^2), \tag{10}$$

due to equilibration of the first equation of (9) to its slow manifold. Indeed, provided $\sigma_\mu = -1$ and $\epsilon \ll 1$, (10) provides the quadratic approximation to a locally attracting (center) manifold [12]. Equivalently, for (2) in the limit $\mu_{1,2} \to 0$ with $\mu_0 \neq 0$, the center manifold tangent to the $a_0 = 0$ hyperplane may be locally approximated by

$$a_0 = -2\sigma_\mu(B_1 a_1^2 + B_2 a_2^2). \tag{11}$$

Substitution of (11) into the latter two equations of (2) yields the reduced system

$$\begin{aligned} \dot{a}_1 &= a_1^* a_2 + (\mu_1 + 2\sigma_\mu B_1^2|a_1|^2 + 2\sigma_\mu B_1 B_2|a_2|^2)a_1 \\ \dot{a}_2 &= -a_1^2 + (\mu_2 + 2\sigma_\mu B_1 B_2|a_1|^2 + 2\sigma_\mu B_2^2|a_2|^2)a_2, \end{aligned} \tag{12}$$

which is precisely the 1:2 resonance system (4), with system parameters

$$e_{11} = 2\sigma_\mu B_1^2, \qquad e_{12} = e_{21} = 2\sigma_\mu B_1 B_2, \qquad e_{22} = 2\sigma_\mu B_2^2. \tag{13}$$

Hence the dynamics of the 0:1:2 resonance (2) are related to those of the *degenerate* 1:2 resonance in which

$$e_{12} = e_{21} = \sigma_\mu \sigma_B \sqrt{e_{11} e_{22}}, \tag{14}$$

where $\sigma_B \stackrel{\text{def}}{=} \text{sign}(B_1 B_2)$ and we implicitly assume $e_{11}e_{22} > 0$. In particular, the fixed point sets of (2) and (12) coincide, as do those of (6) and (8).

This paper is organized as follows. In Section 2 we revisit the general 1:2 resonance of AGH, and then obtain new results for the degenerate 1:2 resonance given by (4) subject to (14). In Section 3 we perform a similar analysis of the 0:1:2 resonance (2). Then in Sections 4 and 5 we examine both spatial resonances with system parameter values representing the two cases noted above, representative of (large) open sets of system parameters. We identify differences between the behavior of the 1:2 and 0:1:2 systems, and find new types of heteroclinic cycles. In Section 6 we relax the assumption that $\mu_0 \neq 0$, and consider the limit $\mu_{0,1,2} \to 0$. This includes a discussion of complicated periodic orbits for the 0:1:2 system. Section 7 concludes the paper.

2. Dynamics of the 1:2 resonance

2.1. Basic solutions

For the reader's convenience, and because we shall describe analogous results for the 0:1:2 system in similar terms, we start by reviewing results which appeared in [2] and [11], summarizing the various solutions to (4) discussed therein. Acronyms for the solution and bifurcation types introduced in this and other sections are given in Table 1.

Trivial state. The solution $a_1 = a_2 = 0$ has full O(2) symmetry and eigenvalues μ_1 and μ_2, each of multiplicity 2.

Pure mode (PM) equilibria. These lie in the $a_1 = 0$ invariant subspace, given by $(a_1, a_2) = (0, \sqrt{-\mu_2/e_{22}}\,e^{2i\bar{\phi}})$ and branch from the origin in a pitchfork bifurcation of revolution along the line $\mu_2 = 0$. For $e_{22} < 0$, as in the degenerate 1:2 resonance when $\sigma_\mu < 0$ (13), PM equilibria exist for $\mu_2 > 0$. These form a circle $\text{PM}_{\bar{\phi}}$ parameterized by $\bar{\phi}$, intersecting the real subspace $y_1 = y_2 = 0$ at the two points PM_0 and $\text{PM}_{\pi/2}$ (given by $(x_1, x_2) = (0, \pm\sqrt{-\mu_2/e_{22}})$).

Table 1
Acronyms for solution and bifurcation types

	Acronym	Full name
Solution type	PM	Pure mode
	MM	Mixed mode
	SW	Standing wave
	TW	Travelling wave
	MTW	Modulated travelling wave
Bifurcation type	SB	Symmetry breaking pitchfork
	H	Hopf
	PB	Parity breaking
	PD	Period doubling
	T	Torus
	SWHe	Heteroclinic involving SW
	SWHo	Homoclinic involving SW
	Sh	Silnikov

Mixed mode (MM) equilibria. These fixed points take the form $(a_1, a_2) = (\pm r_1 e^{i\bar{\phi}}, r_2 e^{2i\bar{\phi}})$, and we shall denote them $\mathrm{MM}^{-}_{\bar{\phi}}$. The non-negative moduli $r_{1,2}$ may be determined from (8) by setting $\phi = 0$ to yield:

$$-\mu_1 + (-1 + e_{21}\mu_1 - e_{11}\mu_2)r_2 + (e_{21} - e_{12})r_2^2 + (e_{12}e_{21} - e_{11}e_{22})r_2^3 = 0, \tag{15}$$

and

$$r_1^2 = -\frac{\mu_1 + r_2 + e_{12}r_2^2}{e_{11}} = \frac{r_2(\mu_2 + e_{22}r_2^2)}{1 - e_{21}r_2}. \tag{16}$$

The first (resp., second) equality in (16) follows from setting $\dot{r}_1 = 0$ (resp., $\dot{r}_2 = 0$) in (8). One might conclude that there may exist at most three distinct (non-symmetry-related) MM states corresponding to the three roots of (15) but, as we shall see in Section 2.2, this is not so in the degenerate case. We note that the MM equilibria bifurcate from the PM equilibria through symmetry-breaking (SB) pitchfork bifurcations. They also bifurcate from the trivial state in a pitchfork of revolution along the line $\mu_1 = 0$.

Standing wave (SW) solutions. These periodic orbits lie in the real subspace or any $\bar{\phi}$-rotation of it, and arise in Hopf (H) bifurcations from the MM equilibria. Linearizing (7), restricting to the real subspace and evaluating the Jacobian matrix at the mixed mode (15)and (16), we obtain the Hopf bifurcation conditions in terms of $r_{1,2}$:

$$0 = -r_1^2 - 2e_{11}r_1^2r_2 - 2e_{22}r_2^3, \tag{17}$$

and

$$(2e_{22}r_2^3 + r_1^2)e_{11} - (2e_{12}r_2 + 1)(e_{21}r_2 - 1)r_2 > 0. \tag{18}$$

Eq. (15) implies that, as $\mu_{1,2} \to 0$, MM solutions with small $r_{1,2}$ must satisfy

$$r_2 \approx -\mu_1. \tag{19}$$

Since r_2 must be non-negative, we conclude that the locus of H bifurcations which limits on the point $\mu = 0$ must locally extend into the $\mu_1 < 0$ half-plane.

In fact, as shown in [1] this locus of H bifurcations is locally parabolic (cf. [2]). Indeed, consider MM solutions with small $r_{1,2}$, corresponding to small μ_1. Assuming $e_{ij} = \mathcal{O}(1)$, $i = 1, 2$, $j = 1, 2$, and using (19), the second term in (17) is small relative to the first. Thus, at a Hopf bifurcation

$$r_1^2 \approx -2e_{22}r_2^3. \tag{20}$$

Furthermore, from the second equality in (16), using (19),

$$r_1^2 \approx r_2(\mu_2 + e_{22}r_2^2). \tag{21}$$

Finally, equating (20) and (21) and using (19),

$$\mu_2 \approx -3e_{22}\mu_1^2. \tag{22}$$

There are also standing wave heteroclinic (SWHe) bifurcations associated with the periodic orbits that are spawned; as such a bifurcation is approached, the periodic orbit limits to connections between the trivial state and a PM solution. We shall use AUTO [13] to map these out in the μ parameter space in the examples considered in Sections 4 and 5.

Travelling wave (TW) solutions. These are fixed points of (6) but periodic orbits for the system (2) with $\dot{\theta}_2 = 2\dot{\theta}_1 \neq 0$. Eq. (8) indicates $2r_2^2 - r_1^2 = 0$ for the travelling waves, and thus

$$\begin{aligned} r_2^2 &= \frac{-(2\mu_1 + \mu_2)}{4e_{11} + 2e_{12} + 2e_{21} + e_{22}}, \qquad r_1 = \sqrt{2}r_2, \\ \cos\phi &= \frac{(2e_{11} + e_{12})\mu_2 - (2e_{21} + e_{22})\mu_1}{\sqrt{-(4e_{11} + 2e_{12} + 2e_{21} + e_{22})(2\mu_1 + \mu_2)}}. \end{aligned} \tag{23}$$

Travelling wave solutions exist in the region of the μ plane defined by

$$((2e_{11} + e_{12})\mu_2 - (2e_{21} + e_{22})\mu_1)^2 \leq -(4e_{11} + 2e_{12} + 2e_{21} + e_{22})(2\mu_1 + \mu_2), \tag{24}$$

and bifurcate from the MM equilibria in parity-breaking (PB) bifurcations when this expression is an equality.

Modulated travelling wave (MTW) solutions. These are created when a Hopf bifurcation occurs in (8), corresponding to a torus (T) bifurcation on a TW branch in the system (4). They may also arise in bifurcations from the SW solutions.

Heteroclinic cycles. In the real (x_1, x_2) subspace these appear as a connection between PM_0 and $\mathrm{PM}_{\pi/2}$. As shown in [2], for parameter values satisfying

$$\mu_1 - \frac{\mu_2 e_{12}}{e_{22}} - \sqrt{\frac{-\mu_2}{e_{22}}} < 0 < \mu_1 - \frac{\mu_2 e_{12}}{e_{22}} + \sqrt{\frac{-\mu_2}{e_{22}}}, \tag{25}$$

PM_0 is a saddle and $\mathrm{PM}_{\pi/2}$ a sink in the real subspace, and a connection between these two equilibria can be proven to exist if there are no MM equilibria present. (The latter condition is sufficient but not necessary: cf. AGH ([2], Figs. 1 and 5).) Given a connection from PM_0 to $\mathrm{PM}_{\pi/2}$, a 'returning' connection in a suitably rotated copy of the real subspace may be found by appeal to O(2) symmetry. More general heteroclinic cycles connecting MM equilibria were shown to exist in the 1:2 resonance in [11].

2.2. The degenerate case

We now consider the degenerate 1:2 resonance (4) with (14), focussing initially on the real subspace, in which the equations reduce to:

$$\begin{aligned} \dot{x}_1 &= x_1 x_2 + (\mu_1 + e_{11}x_1^2 + \sigma_\mu \sigma_B \sqrt{e_{11}e_{22}}x_2^2)x_1, \\ \dot{x}_2 &= -x_1^2 + (\mu_2 + \sigma_\mu \sigma_B \sqrt{e_{11}e_{22}}x_1^2 + e_{22}x_2^2)x_2. \end{aligned} \tag{26}$$

Focussing on the MM equilibrium condition (15) specialized to the real subspace, we see that the quadratic and cubic terms vanish identically and it simplifies to:

$$-\mu_1 + (-1 + \sigma_\mu \sigma_B \sqrt{e_{11}e_{22}}\mu_1 - e_{11}\mu_2)x_2 = 0. \tag{27}$$

One might be tempted to rearrange this equation to read

$$x_2 = \frac{\mu_1}{-1 + \sigma_\mu \sigma_B \sqrt{e_{11} e_{22}} \mu_1 - e_{11} \mu_2}, \tag{28}$$

and then conclude that $\mu_1 \to 0$ necessarily implies $x_2 \to 0$ (and hence, from (16), $x_1 \to 0$) also. This holds on all parameter space paths approaching the $\mu_1 = 0$ axis, *except* those that approach the point

$$\mu = (0, -1/e_{11}) \stackrel{\text{def}}{=} \tilde{\mu}, \tag{29}$$

where the denominator of (28) vanishes. The PM equilibria undergo SB pitchfork bifurcations to MM equilibria on such a path, which can be found by setting $(r_1, r_2) = (0, \sqrt{-\mu_2/e_{22}})$ in (16) and using (14) to obtain

$$\left(\mu_1 - \sigma_\mu \sigma_B \sqrt{\frac{e_{11}}{e_{22}}} \mu_2 \right)^2 = -\frac{\mu_2}{e_{22}} \tag{30}$$

We shall defer discussion of this parabola until Section 3.1 where we discuss the MM equilibria in the 0:1:2 resonance which, as we observed in Section 1, are found to lie at identical values of (a_1, a_2). For now, we note that if we solve (30) for μ_2 as a function of μ_1 and substitute this relation back into (28), we can apply L'Hopital's rule to conclude that, along this curve, x_2 remains equal to $\pm\sqrt{-\mu_2/e_{22}}$ as $\mu_1 \to 0$.

A second path approaching (29) is the curve on which MM equilibria undergo H bifurcations. We concluded in Section 2.1 that, for $e_{11}, e_{22} < 0$, the H bifurcation curve enters the $\mu_1 < 0$ half-plane from $\mu = 0$. If it is subsequently to approach the $\mu_1 = 0$ axis it may only do so at the point $\mu_2 = -1/e_{11}$; at all other points the MM equilibria coalesce at the origin, at which a H bifurcation cannot take place, since the $x_1 = 0$ axis is invariant. We may confirm this reasoning and explore the bifurcations by considering equilibria of (26) at the parameter values (29), which lie on the set

$$e_{11} x_1^2 + \sigma_\mu \sigma_B \sqrt{e_{11} e_{22}}\, x_2^2 + x_2 = 0. \tag{31}$$

Hence for $\sigma_\mu \sigma_B < 0$ a closed curve of equilibria passes through both $(x_1, x_2) = (0, 0)$ and the PM equilibrium $(x_1, x_2) = (0, -\sigma_\mu/\sqrt{e_{11} e_{22}}) = (0, -\sigma_\mu \sqrt{-\mu_2/e_{22}})$. For $\sigma_\mu \sigma_B > 0$ two curves of equilibria exist, one passing through $(0, 0)$, and the other through the PM equilibrium $(0, \sigma_\mu/\sqrt{e_{11} e_{22}}) = (0, \sigma_\mu \sqrt{-\mu_2/e_{22}})$; if $\sigma_\mu < 0$, as in the two examples considered in Sections 4 and 5, these two PM equilibria are none other than PM_0 and $PM_{\pi/2}$, respectively. See Figs. 5 and 16 below.

Linearization of (26) on the set (31) yields eigenvalues

$$\lambda = 0, -\frac{1 + \sigma_\mu \sigma_B \sqrt{e_{11} e_{22}} x_2 + 2 e_{11} x_2 (1 - e_{22} x_2 + \sigma_\mu \sigma_B \sqrt{e_{11} e_{22}})}{e_{11}}, \tag{32}$$

and eigenvectors

$$\left(\mp \frac{1 + 2\sigma_\mu \sigma_B \sqrt{e_{11} e_{22}} x_2}{2\sqrt{-e_{11} x_2 (1 + \sigma_\mu \sigma_B \sqrt{e_{11} e_{22}} x_2)}}, 1 \right), \quad \left(\mp \frac{\sqrt{-e_{11} x_2 (1 + \sigma_\mu \sigma_B \sqrt{e_{11} e_{22}} x_2)}}{1 - \sigma_\mu \sigma_B \sqrt{e_{11} e_{22}} x_2}, 1 \right). \tag{33}$$

The former, with zero eigenvalue, is tangent to the curve (31) and the second eigenvalue is also zero when

$$x_2 = x_2^{\text{TB}} \stackrel{\text{def}}{=} \frac{2e_{11} + \sigma_\mu \sigma_B \sqrt{e_{11} e_{22}} \pm \sqrt{e_{11} (4e_{11} - 4\sigma_\mu \sigma_B \sqrt{e_{11} e_{22}} + 9 e_{22})}}{4 e_{11} (e_{22} - \sigma_\mu \sigma_B \sqrt{e_{11} e_{22}})}, \tag{34}$$

at which point the Jacobian matrix of (26) takes the form:

$$\begin{bmatrix} -a & b \\ -\dfrac{a^2}{b} & a \end{bmatrix}, \tag{35}$$

where a and b are complicated functions of e_{11} and e_{22}. The corresponding pair of equilibria $x^{\mathrm{TB}} \stackrel{\mathrm{def}}{=} (x_1^{\mathrm{TB}}, x_2^{\mathrm{TB}})$ are degenerate Takens-Bogdanov bifurcation points, as one sees by putting the linear part (35) into Jordan form and applying a near-identity normal form transformation to remove all but the essential quadratic terms [12]. The generic Takens-Bogdanov singularity has two such, but in the present case one of them identically vanishes, giving (in Bogdanov form):

$$\begin{aligned} \dot{u}_1 &= u_2, \\ \dot{u}_2 &= \pm u_1 u_2 + \cdots. \end{aligned} \tag{36}$$

This lacks the u_1^2 term that is generically present [12], as it must, consistent with existence of the curve of equilibria (31): see Fig. 5 below. In (36) this curve is transformed to coincide with the u_1-axis and all other solutions lie on the parabolae $u_2 = \text{const.} \pm u_1^2/2$. The sign of the u_1u_2 term is determined by the system parameters e_{11}, e_{22}, and hence, via (13), B_1 and B_2. Details of the similarity and normal form transformations, and the (very long) expression for the u_1u_2 coefficient, derived using Mathematica, may be obtained from the first author.

As in the codimension-2 Takens-Bogdanov bifurcation, a locus of H bifurcations emanates from this point; however, *unlike* the standard case, a locus of SWHe bifurcations replaces the homoclinic bifurcations: these are none other than the H and SWHe loci of Section 2.1 that limit on $\mu = 0$. For $\sigma_\mu\sigma_{\mathrm{B}} < 0$ exactly one value of x_2^{TB} will be positive whenever $0 > e_{11} > e_{22}$, in which case all equilibria on the curve (31) with $0 < x_2 < x_2^{\mathrm{TB}}$ (resp., $0 < x_2^{\mathrm{TB}} < x_2$) will be unstable (resp., stable).

One may easily check that the point (29) also belongs to the set along which TW solutions bifurcate from the MM equilibria through PB bifurcations; in the degenerate case, this set, determined by the condition that (24) is an equality, may be written

$$((2e_{11} + \sigma_\mu\sigma_{\mathrm{B}}\sqrt{e_{11}e_{22}})\mu_2 - (2\sigma_\mu\sigma_{\mathrm{B}}\sqrt{e_{11}e_{22}} + e_{22})\mu_1)^2 = -(2\sqrt{e_{11}} + \sigma_\mu\sigma_{\mathrm{B}}\sqrt{e_{22}})^2(2\mu_1 + \mu_2). \tag{37}$$

There are thus two additional distinguished points x^{PB} on (one of) the curves of equilibria (31) where, in accordance with (23), $x_1 = \pm\sqrt{2}x_2$, at which MM equilibria bifurcate to TW solutions; from (31) we easily see these to be the points

$$(x_1^{\mathrm{PB}}, x_2^{\mathrm{PB}}) = \left(\mp \frac{\sqrt{2}}{e_{11}(2 + \sigma_\mu\sigma_{\mathrm{B}}\sqrt{e_{22}/e_{11}})}, -\frac{1}{e_{11}(2 + \sigma_\mu\sigma_{\mathrm{B}}\sqrt{e_{22}/e_{11}})} \right), \tag{38}$$

We shall see examples of the theory expounded in this section in Sections 4.1 and 5.1.

3. Dynamics of the 0:1:2 resonance

3.1. Basic solutions

As noted in Section 1, the (a_1, a_2) coordinates of fixed points of the 0:1:2 and degenerate 1:2 systems coincide. We now re-examine these points in (2) to determine the effects of the extra (a_0) dimension, which can provide an additional direction for instabilities. The PM equilibria of the 1:2 resonance are replaced by ones of the form

$(a_0, 0, a_2)$, and the MM equilibria by (a_0, a_1, a_2), with all $a_j \neq 0$. We shall continue to refer to them, respectively, as pure (albeit now with two nonzero coordinates) and mixed.

Trivial state. The solution $a_j = 0$ has full O(2) symmetry and eigenvalues μ_0, μ_1 and μ_2, the latter two each having multiplicity 2.

Pure mode (PM) equilibria. These lie on the circle $\mathrm{PM}_{\bar{\phi}}$ given by

$$(a_0, a_1, a_2) = \left(\frac{\mu_2}{B_2}, 0, \sqrt{\frac{-\mu_2\sigma_\mu}{2B_2^2}} \mathrm{e}^{2\mathrm{i}\bar{\phi}} \right), \tag{39}$$

which intersects the real subspace at the points PM_0 and $\mathrm{PM}_{\pi/2}$:

$$(a_0, x_1, x_2) = \left(\frac{\mu_2}{B_2}, 0, \pm\sqrt{\frac{-\mu_2\sigma_\mu}{2B_2^2}} \right). \tag{40}$$

Linearizing (5) at these points we obtain the eigenvalues and eigenvectors

$$\begin{aligned}
\lambda_1 &= \frac{(\sigma_\mu + \sqrt{1 - 16B_2^2x_2^2})}{2} = \frac{(\sigma_\mu + \sqrt{1 + 8\sigma_\mu\mu_2})}{2},\\
\lambda_4 &= \frac{(\sigma_\mu - \sqrt{1 - 16B_2^2x_2^2})}{2} = \frac{(\sigma_\mu - \sqrt{1 + 8\sigma_\mu\mu_2})}{2},\\
\lambda_2 &= \mu_1 - B_1a_0 + x_2 = \mu_1 - B_1\mu_2/B_2 + \frac{g\sqrt{-\sigma_\mu\mu_2}}{\sqrt{2B_2^2}},\\
\lambda_3 &= \mu_1 - B_1a_0 - x_2 = \mu_1 - B_1\mu_2/B_2 - \frac{g\sqrt{-\sigma_\mu\mu_2}}{\sqrt{2B_2^2}},\\
\lambda_5 &= \mu_2 - B_2a_0 = 0,
\end{aligned} \tag{41}$$

$$\begin{aligned}
v_1 &= ((-\sigma_\mu - \sqrt{1 + 8\sigma_\mu\mu_2})\frac{g}{\sqrt{-2\sigma_\mu\mu_2}}, 0, 0, 1, 0)^{\mathrm{T}},\\
v_4 &= ((-\sigma_\mu + \sqrt{1 + 8\sigma_\mu\mu_2})\frac{g}{\sqrt{-2\sigma_\mu\mu_2}}, 0, 0, 1, 0)^{\mathrm{T}},\\
v_2 &= (0, 1, 0, 0, 0)^{\mathrm{T}},\\
v_3 &= (0, 0, 1, 0, 0)^{\mathrm{T}},\\
v_5 &= (0, 0, 0, 0, 1)^{\mathrm{T}},
\end{aligned} \tag{42}$$

where $g = 1$ for PM_0 and $g = -1$ for $\mathrm{PM}_{\pi/2}$. We observe that the v_1, v_4 eigenpair span the (a_0, x_2) plane provided $1 + 8\sigma_\mu\mu_2 \neq 0$.

Mixed mode (MM) equilibria. These equilibria, again denoted $\mathrm{MM}_{\bar{\phi}}$, take the form $(a_0, \pm r_1\mathrm{e}^{\mathrm{i}\bar{\phi}}, r_2\mathrm{e}^{2\mathrm{i}\bar{\phi}})$, where

$$\begin{aligned}
a_0 &= \frac{2\mu_1(\mu_2B_1 - \mu_1B_2)}{\sigma_\mu + 2B_1(\mu_2B_1 - \mu_1B_2)},\\
r_1 &= \frac{\sqrt{-\sigma_\mu\mu_1[\sigma_\mu\mu_2 + 2(\mu_2B_1 - \mu_1B_2)^2]}}{\sigma_\mu + 2B_1(\mu_2B_1 - \mu_1B_2)},\\
r_2 &= \frac{-\sigma_\mu\mu_1}{\sigma_\mu + 2B_1(\mu_2B_1 - \mu_1B_2)}.
\end{aligned} \tag{43}$$

The second expression of (43) reveals that MM equilibria exist when

$$\sigma_\mu \mu_1 [2(\mu_1 B_2 - \mu_2 B_1)^2 + \sigma_\mu \mu_2] \leq 0, \tag{44}$$

and these equilibria branch from PM equilibria in SB pitchfork bifurcations along a parabola where (44) vanishes:

$$\mu_1 = \frac{\mu_2 B_1 \pm \sqrt{-\sigma_\mu \mu_2/2}}{B_2}. \tag{45}$$

(Recalling (13), (45) coincides with (30).) This parabola exists for positive (resp., negative) values of μ_2 when $\sigma_\mu = -1$ (resp., $\sigma_\mu = +1$) and has an extremum at

$$\mu_1 = \frac{\sigma_\mu}{8 B_1 B_2}; \tag{46}$$

since it must pass through $\mu = 0$, it is therefore unbounded in the right (resp., left) half-plane for $\sigma_\mu B_2 < 0$ (resp., $\sigma_\mu B_2 > 0$) (recall we assume $B_1 > 0$). From (44), the MM equilibria exist inside (resp., outside) the parabola whenever $\sigma_\mu \mu_1 > 0$ (resp., $\sigma_\mu \mu_1 < 0$). MM equilibria also bifurcate from the trivial state in a pitchfork of revolution along the line $\mu_1 = 0$: see §3.2.

Further consideration of (43) reveals that the MM equilibria tend to infinity as μ approaches the line

$$\mu_1 = \frac{B_1}{B_2}\mu_2 + \frac{\sigma_\mu}{2 B_1 B_2}, \tag{47}$$

which coincides with an analogous expression that can be derived for the degenerate 1:2 resonance. This line intersects (45) at

$$\tilde{\mu} = \mu = \left(0, \frac{-\sigma_\mu}{2B_1^2}\right) = \left(0, \frac{-1}{e_{11}}\right). \tag{48}$$

and intersects the region where MM equilibria exist when $B_2 < 0$, i.e. $\sigma_B < 0$, and not otherwise. Examples follow in Sections 4 and 5. This bifurcation from infinity is an artifact of the quadratic truncation in (1).

Standing wave (SW) solutions. Due to the extra (a_0) dimension, these periodic orbits are much more difficult to locate in the 0:1:2 resonance than their counterparts in the degenerate 1:2 resonance. Numerical branch following using AUTO [13] will reveal differences from the degenerate 1:2 resonance, including period-doubling (PD) bifurcations, standing wave homoclinic (SWHo), and Silnikov (Sh) bifurcations [12]. The fixed points involved in the SWHo and Sh bifurcations are typically MM solutions.

Travelling wave (TW) solutions. These are fixed points of (8) but periodic orbits of (4) with $\dot{\theta}_2 = 2\dot{\theta}_1 \neq 0$. They satisfy

$$r_2^2 = \frac{-\sigma_\mu(2\mu_1 + \mu_2)}{2(2B_1 + \sigma_B B_2)^2}, \qquad r_1 = \sqrt{2} r_2, \qquad a_0 = -2\sigma_\mu(B_1 r_1^2 + B_2 r_2^2),$$

$$\cos\phi = \frac{\sqrt{2}\sigma_\mu[(2B_1^2 + \sigma_B B_1 B_2)\mu_2 - (2\sigma_B B_1 B_2 + B_2^2)\mu_1]}{\sqrt{-(2B_1 + \sigma_B B_2)^2(2\mu_1 + \mu_2)}},$$

and exist for parameter values such that

$$2[(2B_1^2 + \sigma_B B_1 B_2)\mu_2 - (2\sigma_B B_1 B_2 + B_2^2)\mu_1]^2 \leq -(2B_1 + \sigma_B B_2)^2(2\mu_1 + \mu_2), \tag{49}$$

(equivalent to (24) via (13)). They appear in PB bifurcations from the MM equilibria when (49) is an equality. The parabola describing the PB bifurcations has an extremum at

$$\mu = \left(\frac{\sigma_\mu}{8B_1(2B_1 + B_2)}, \frac{-\sigma_\mu(4B_1 + B_2)}{8B_1^2(2B_1 + B_2)}\right) \tag{50}$$

which, for $\sigma_\mu > 0$ lies in the $\mu_1 < 0$, $\mu_2 > 0$ quadrant when $B_1 > -2B_2$ and the $\mu_1 > 0$, $\mu_2 < 0$ quadrant for $B_1 < -2B_2$, and includes the point $\mu = \tilde{\mu}$ as defined in (29).

Modulated travelling wave (MTW) solutions. These are created when a H bifurcation occurs in (6), corresponding to a torus (T) bifurcation on a TW branch in (2). The examples to follow show that the MTW bifurcation sets for the degenerate 1:2 and 0:1:2 systems are *not* coincident.

Heteroclinic cycles of AGH type. Structurally stable heteroclinic cycles, analogous to those of [2] noted in Section 2.1, also occur for the 0:1:2 system. Up to an estimate that must be checked numerically, we can prove their existence as follows. As in [2] we restrict to the real subspace, assume that $\sigma_\mu = -1$ and $\mu_2, B_1, B_2 > 0$, and demonstrate the existence of a connection between the PM_0 and $\mathrm{PM}_{\pi/2}$ equilibria, the return part of the cycle being guaranteed by O(2) symmetry.

To obtain the necessary stability types for a connection (i.e. PM_0 has a one-dimensional unstable manifold and $\mathrm{PM}_{\pi/2}$ is a sink in the real subspace), from (41) and (42) we require that

$$\mu_1 B_2 - \mu_2 B_1 + \sqrt{\frac{\mu_2}{2}} > 0 > \mu_1 B_2 - \mu_2 B_1 - \sqrt{\frac{\mu_2}{2}}, \tag{51}$$

which, via (13), coincides with the existence conditions of AGH ([2], Theorem 3.2). (The other eigenvalues corresponding to perturbations in the real subspace are guaranteed to have negative real part since $\mu_2 > 0$.) Attractivity of the cycles (in the full phase space) is guaranteed by requiring that the real part of the least stable eigenvalue for $\mathrm{PM}_{\pi/2}$ has larger magnitude than the magnitude of the (real) unstable eigenvalue for PM_0. This corresponds to

$$\min\left\{\left|\mathcal{R}\left(B_2\frac{(-1+\sqrt{1-8\mu_2})}{2}\right)\right|, -\left(\mu_1 B_2 - \mu_2 B_1 - \sqrt{\frac{\mu_2}{2}}\right)\right\} > \mu_1 B_2 - \mu_2 B_1 + \sqrt{\frac{\mu_2}{2}}. \tag{52}$$

Here $\mathcal{R}$ denotes the real part of the quantity in parenthesis.

We first observe that the set

$$Q^- \stackrel{\text{def}}{=} \{(a_0, x_1, x_2) | a_0 > 0, x_2 < 0\},$$

with boundaries

$$\partial Q_1^- \stackrel{\text{def}}{=} \{(a_0, x_1, x_2) | a_0 > 0, x_2 = 0\}, \quad \partial Q_2^- \stackrel{\text{def}}{=} \{(a_0, x_1, x_2) | a_0 = 0, x_2 < 0\}$$

and containing $\mathrm{PM}_{\pi/2}$, is positively invariant. This is easily seen since, from the fourth equation of (5), $\dot{x}_2 = -x_1^2 < 0$ on ∂Q_1^-, while the first of (5) implies that $\dot{a}_0 = 2(B_1 x_1^2 + B_2 x_2^2) > 0$ on ∂Q_2^- except at the trivial equilibrium.

We next assert that any solution which enters Q^- approaches the plane $x_1 = 0$. On the real subspace we have $\dot{x}_1 = (\mu_1 - B_1 a_0 + x_2)x_1$, and, for $B_1 > 0$, $\mu_1 - B_1 a_0 + x_2 \leq \mu_1$. Hence, for $\mu_1 < 0$, x_1 must decay exponentially to zero (this may also occur for $\mu_1 > 0$ in certain regions of phase space; cf. Fig. 2). The flow on the (a_0, x_2) plane is given by

$$\begin{aligned} \dot{a}_0 &= \sigma_\mu a_0 + 2B_2 x_2^2 \\ \dot{x}_2 &= (\mu_2 - B_2 a_0)x_2, \end{aligned} \tag{53}$$

whose phase portrait is shown in Fig. 1.

To verify this picture, we note that the origin is globally asymptotically stable for $\sigma_\mu, \mu_2 < 0$, since $\dot{E} = \sigma_\mu a_0^2 + \mu_2 x_2^2 < 0$ for $a_0, x_2 \neq 0$ (cf. Eq. (3)). As μ_2 increases through 0, the pure modes PM_0, $\mathrm{PM}_{\pi/2}$ bifurcate from the origin and a center manifold analysis [12] reveals that they are the sole limit sets, excepting the origin, for $0 < \mu_2 \ll 1$. They remain sinks for all $\mu_2 > 0$, but periodic or homoclinic orbits surrounding them could appear in global bifurcations. However, since the flow far from the origin is dominated by the integrable quadratic system, for which all solutions excepting the invariant a_0-axis move upwards along ellipses $a_0^2/2 + x_2^2 = \text{const.}$, no bifurcations

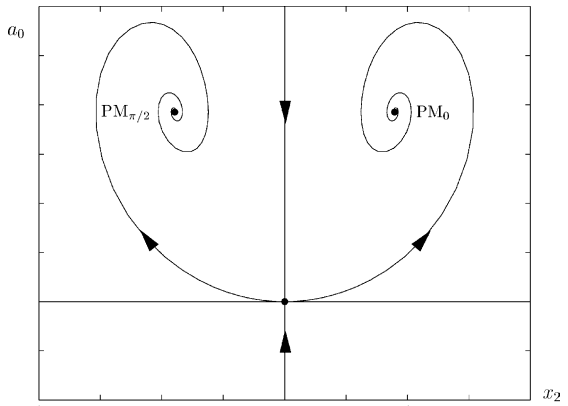

Fig. 1. Phase portrait of (53) for $\sigma_\mu = -1$, $\mu_2 > 0$, $B_2 > 0$.

from infinity can occur for $\mu_2 > 0$, and since $W^{\mathrm{s}}(0,0)$ is the a_0-axis, no 'finite' homoclinic bifurcation can occur either. We have been unable to rule out the possible creation of periodic orbits surrounding PM_0, $\mathrm{PM}_{\pi/2}$ in saddle-node bifurcations, but careful studies of null- and isoclines, and extensive numerical work, suggest that Fig. 1 is correct for all $\mu_2 > 0$. This implies that any trajectory approaching the $x_1 = 0$ plane inside Q^- limits on $\mathrm{PM}_{\pi/2}$ as $t \to \infty$.

Assuming that periodic orbits are not born in saddle-node bifurcations, we need only show that the unstable manifold of PM_0 $W^{\mathrm{u}}(\mathrm{PM}_0)$ intersects ∂Q_1^-. We define a set containing PM_0 by

$$Q^+ \stackrel{\mathrm{def}}{=} \{(a_0, x_1, x_2) | a_0 > 0, x_2 > 0\},$$

within which there exists a manifold on which $\dot{x}_2 = 0$:

$$M \stackrel{\mathrm{def}}{=} \left\{ (a_0, x_1, x_2) | a_0 = \frac{\mu_2}{B_2} - \frac{x_1^2}{B_2 x_2}, a_0 > 0, x_2 > 0 \right\}. \tag{54}$$

In (a_0, x_1, x_2) space M has the appearance of a ship's bow with the line $a_0 = \mu_2/B_2$, $x_1 = 0$ forming the prow. Points 'outside' (resp., 'inside') of the 'bow' have $\dot{x}_2 < 0$ (resp., $\dot{x}_2 > 0$). Clearly PM_0 lies on M, and its eigenvectors (42), show that $W^{\mathrm{u}}(\mathrm{PM}_0)$ is normal to the (a_0, x_2) plane at PM_0, and thus enters the region where $\dot{x}_2 < 0$. Hence x_2 initially decreases and will continue to do so until the orbit crosses ∂Q_1^-, provided that $W^{\mathrm{u}}(\mathrm{PM}_0)$ does not subsequently intersect M. We have been unable to prove this, although numerical simulations suggest that it holds. We show an example in Fig. 2.

3.2. Special solutions at $\mu = \tilde{\mu}$

Eq. (43) implies that the MM equilibria for the 0:1:2 resonance also converge on the origin as $\mu_1 \to 0$, except at the point $\mu = \tilde{\mu}$ as given by (48), where the locus of SB bifurcations (45) crosses the $\mu_1 = 0$ axis. Here, the real equations take the form

$$\begin{aligned} \dot{a}_0 &= \sigma_\mu a_0 + 2(B_1 x_1^2 + B_2 x_2^2), \\ \dot{x}_1 &= -B_1 a_0 x_1 + x_1 x_2, \\ \dot{x}_2 &= \left(\frac{-\sigma_\mu}{2B_1^2} - B_2 a_0 \right) x_2 - x_1^2, \end{aligned} \tag{55}$$

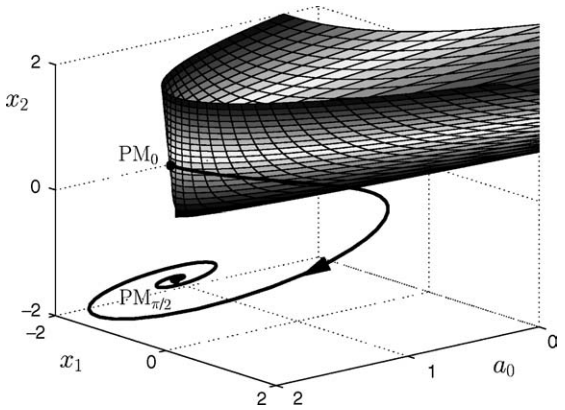

Fig. 2. Heteroclinic connection between the PM_0 and $\mathrm{PM}_{\pi/2}$ equilibria for the parameters $(\mu_1, \mu_2, B_1, B_2) = (0.0745, 2.318, 0.4375, 1.2031)$. The heteroclinic trajectory (bold) lies below M (shaded), given by (54). Note that $\mu_1 > 0$ here. We shall refer to this example again in Section 4.2.

and hence we have either one or two sets of equilibria given by

$$\begin{aligned} x_1 &= \frac{\pm\sqrt{-x_2(\sigma_\mu + 2B_1B_2x_2)}}{\sqrt{2}B_1}, \\ a_0 &= \frac{x_2}{B_1}. \end{aligned} \tag{56}$$

The locus (56) coincides with that of (31) when projected onto the (x_1, x_2) plane, and passes through the trivial equilibrium as well as the point

$$(a_0, x_1, x_2) = \left(\frac{-\sigma_\mu}{2B_1^2B_2}, 0, \frac{-\sigma_\mu}{2B_1B_2}\right). \tag{57}$$

For $B_2 > 0$ there is one closed curve of equilibria passing through these points, while for $B_2 < 0$ there are two hyperbolae, one of which passes through the trivial equilibrium whilst the other passes through (57).

The eigenvalues on the curve of equilibria (56) are

$$\lambda_1 = 0, \qquad \lambda_{2,3} = \frac{\tilde{\lambda} \pm \sqrt{\hat{\lambda}}}{4B_1^2} \tag{58}$$

where

$$\tilde{\lambda} = \sigma_\mu(p-2) - 2B_1B_2x_2, \tag{59}$$

$$\hat{\lambda} = p^2 + 4B_1p(4B_1 + B_2)x_2\sigma_\mu + 4B_1^2B_2(B_2 + 8B_1(p - 2B_1B_2))x_2^2, \tag{60}$$

$$p = 1 + 2B_1^2. \tag{61}$$

There are two zero eigenvalues when one of $\tilde{\lambda} \pm \sqrt{\hat{\lambda}}$ vanishes; this occurs at

$$x_2 = \frac{-\sigma_\mu(p + B_1B_2) \pm \sqrt{p^2 - 2B_1B_2p + 9B_1^2B_2^2}}{4B_1B_2(p - 2B_1B_2)}. \tag{62}$$

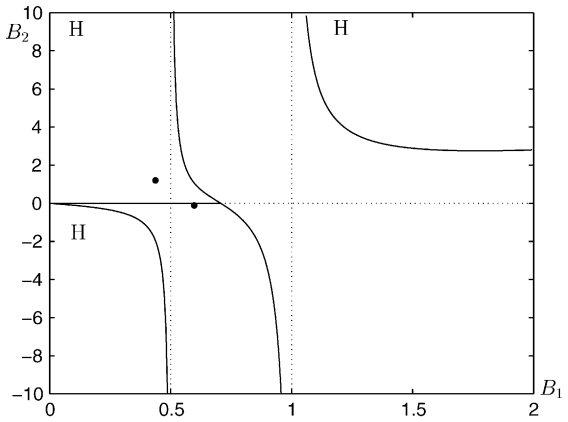

Fig. 3. Regions of (B_1, B_2) space where condition (64) is satisfied are labeled 'H' and bounded by solid lines and figure axes.

and is analogous to x^{TB} in the degenerate 1:2 resonance. However, rather than being the limit of a locus of H and associated SWHe bifurcations, we find that an SWHo bifurcation is more commonly encountered at this point.

Further consideration of the eigenvalues (58) shows that the H locus emanating from $\mu = 0$ may pass through $\mu = \tilde{\mu}$. For this we require $\tilde{\lambda} = 0$ and $\hat{\lambda} < 0$, or

$$x_2 = \sigma_\mu \frac{p-2}{2B_1B_2}, \tag{63}$$

and

$$\frac{B_1 p(p-2) - B_2(4B_1^2 - 1)(B_1^2 - 1)}{B_2} < 0. \tag{64}$$

For the case $\sigma_\mu < 0$ and $B_2 > 0$, a pair of points satisfy (63) on the (single) curve of equilibria provided $0 \le B_1 \le 1/\sqrt{2}$. For $\sigma_\mu < 0$ and $B_2 < 0$, a pair of points on the upper ($x_2 > 0$) of the two curves satisfy (63) provided $B_1 > 1/\sqrt{2}$.

The condition (64) is somewhat more restrictive, however. Fig. 3 shows regions of system parameter space in which this condition holds, the points $(B_1, B_2) = (0.4375, 1.2031)$ and $(B_1, B_2) = (0.5974, -0.1149)$, corresponding to the examples of Sections 4 and 5 being indicated by solid dots. In the latter case the H bifurcation curve emanating from $\mu = 0$ cannot pass through $\mu = \tilde{\mu}$.

4. Example 1: $B_1 = 0.4375$, $B_2 = 1.2031$, $\sigma_\mu = -1$

We now give two examples of the degenerate 1:2 and 0:1:2 resonances for specific system parameters $B_{1,2}$. This first, representative of the case $\sigma_\mu = -1$ and $B_1, B_2 > 0$, is taken from our previous study of low-dimensional models of plane Couette flow in a moderate aspect ratio domain [3], where it appeared as a projection of the Navier-Stokes equations onto empirically obtained modes with spanwise wavenumbers in the ratio 0:1:2. In [3], a_0 represents the amplitude of a mean flow mode and a_1 and a_2 the amplitudes of streamwise-invariant vortical modes and their dynamics for these parameter values, particularly the heteroclinic cycles considered in Section 3.1, explains why streamwise vortices are prominent features in turbulent PCF despite being linearly unstable.

4.1. Degenerate 1:2 resonance

In this case the 1:2 system parameter values are

$$e_{11} = -0.3828, \quad e_{12} = e_{21} = -1.0527, \quad e_{22} = -2.8950. \tag{65}$$

Since $\sigma_\mu = -1$ and $B_2 > 0$, the parabola (45) on which SB bifurcations from PM to MM equilibria occur lies entirely in the $\mu_2 \geq 0$ half-plane and, from (46), its extremum lies in the $\mu_1 < 0$, $\mu_2 > 0$ quadrant. The parabola of PB bifurcations exists for all μ_2, and from (24) also has its extremum in the $\mu_1 < 0$, $\mu_2 > 0$ quadrant. These curves, as well as similar parabolas of T, H and SWHe bifurcations numerically computed via AUTO, are shown in Fig. 4.

In accord with the analysis of Section 3, the H bifurcation curve enters the $\mu_1 < 0$ half-plane and later turns around to limit on $\mu = \tilde{\mu} = (0, -1/e_{11}) = (0, 2.6122)$; as we move along this curve and μ approaches this point from the left, the pair of MM equilibria at which H bifurcations occur tend towards $(x_1, x_2) \approx (\pm 0.7815, 0.4158)$, in agreement with the coordinates of the Takens-Bogdanov point given by (31), combined with the '+' solution of (34) (we may exclude the '−' solution since it is negative and therefore cannot satisfy (17)). The curve of equilibria (31) is shown in Fig. 5, with the Takens-Bogdanov points indicated. Two loci of T bifurcations from TW to MTW also leave $\mu = 0$; one of these limits on $\mu = \tilde{\mu}$; the other enters the $\mu_1 > 0$ half-plane and tends to infinity.

We now consider the behavior of solutions to (4) subject to (65) as μ_1 varies with μ_2 fixed. As μ_1 increases for $\mu_2 \in (0, -1/e_{11})$, an SB bifurcation is first encountered in which PM equilibria lose stability to MM equilibria; depending on the value of μ_2, H, SWHe or PB bifurcation sets may be crossed next. For $\mu_2 = 0.5$, the sequence is SB → H → SWHe → PB → T, as shown in the bifurcation diagram of Fig. 6. Here MM equilibria are born in a SB bifurcation at $\mu_1 \approx -0.2338$; they remain stable until $\mu_1 \approx -0.1391$ where they undergo a H bifurcation to stable SW solutions. The latter exist over a small range of parameter space, before being destroyed in a SWHe bifurcation at $\mu_1 \approx -0.1329$, in which stable heteroclinic cycles appear. As μ_1 further increases, unstable TW solutions are born in a PB bifurcation at $\mu_1 \approx -0.1190$; these grow in amplitude while the unstable MM equilibria converge on the origin as $\mu_1 \to 0^-$. The TW gain stability in a T bifurcation at $\mu_1 \approx 0.0854$ that produces unstable MTW solutions. The heteroclinic cycles appear to remain stable until $\mu_1 \approx 0.177$, corresponding to a global bifurcation in which the MTWs coalesce with them (cf. [2], §5), although we were unable to follow the MTWs beyond $\mu_1 \approx 0.1762$.

For higher values of μ_2 the bifurcation sequence, after the initial SB bifurcation, may be any of H → PB → SWHe → T, PB → T → H → BP → SWHe → T, PB → H → T → SWHe → T or PB → H → SWHe → T. A representative example of the first occurs for $\mu_2 = 0.9$, which yields a bifurcation diagram qualitatively similar to

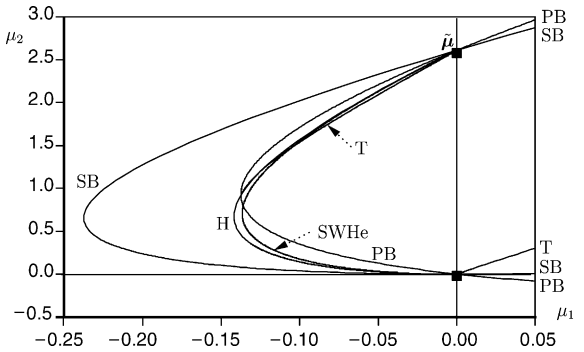

Fig. 4. Various bifurcation sets for (4) with $e_{11} = -0.3828$, $e_{12} = e_{21} = -1.0527$, and $e_{22} = -2.8950$ featuring symmetry-breaking (SB) pitchfork, Hopf (H), standing wave heteroclinic (SWHe), parity-breaking (PB) and torus (T) bifurcations. The H, SWHe and T curves are difficult to distinguish in the upper half of this figure.

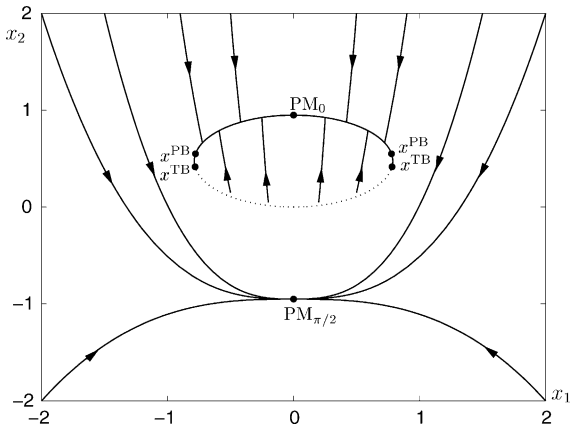

Fig. 5. Phase space of (26) for system parameters (65) at $\mu = \tilde{\mu}$ with sample trajectories. PM_0 and $\mathrm{PM}_{\pi/2}$ denote the pure mode equilibria and points at which Takens-Bogdanov and parity-breaking bifurcations occur are are labelled x^{TB} and x^{PB}, respectively.

that in Fig. 6, with the SW solution branch extending further to the right beyond the PB bifurcation point. We do not show this.

The case $\mu_2 = 1.0$ exemplifies the second of these sequences: Fig. 7. Here, after being spawned in a SB bifurcation at $\mu_1 \approx -0.2241$, the stable MM equilibria lose stability in a PB bifurcation to stable TWs at $\mu_1 \approx -0.1371$, and subsequently undergo a H bifurcation to unstable SW solutions at $\mu_1 \approx -0.1345$. Meanwhile, the stable TWs undergo a T bifurcation to stable MTWs at $\mu_1 \approx -0.1349$. The unstable SW and stable MTWs meet in a branch point (BP) of periodic orbits at $\mu_1 \approx -0.1315$, after which the MTWs are extinguished and stable SWs remain until destroyed in a SWHe bifurcation at $\mu_1 \approx -0.1310$.

Examples of bifurcation diagrams showing the third and fourth sequences listed above may be found in [14].

4.2. 0:1:2 Resonance

We next turn to the full system (2) with the same system parameters. For reasons given previously, the SB and PB bifurcation curves are identical to those found in Section 4.1. We again turn to AUTO to compute the loci of H, SWHe and T bifurcation sets departing from $\mu = 0$; the results are given in Fig. 8. We observe two distinct H bifurcation branches: one leaves the origin with $\mu_1 < 0$, $\mu_2 > 0$ (cf. (22)) and then *passes through* $\mu = \tilde{\mu}$ into the

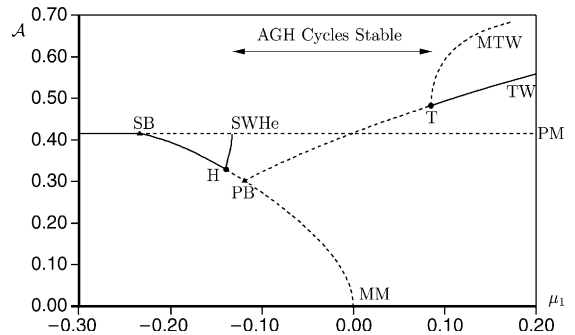

Fig. 6. Bifurcation diagram for (26) with system parameters (65) and $\mu_2 = 0.5$. Here and on subsequent bifurcation diagrams, stable branches are shown solid and unstable branches dashed. Also, here and on other bifurcation diagrams for the degenerate 1:2 mode interaction, $\mathcal{A} = \sqrt{\max(|a_1|^2 + |a_2|^2)}$, where, for periodic orbits, $\max(\cdot)$ denotes the maximum value attained over one period.

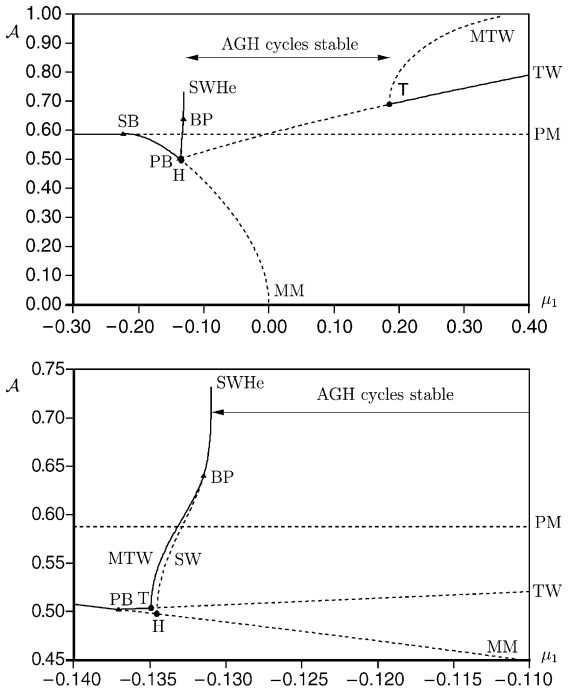

Fig. 7. Bifurcation diagram for (26) with system parameters (65) and $\mu_2 = 1.0$. Region near PB shown in blow up on lower panel.

$\mu_{1,2} > 0$ quadrant (and subsequently through the right boundary of Fig. 8). A second branch originates at $\mu = \tilde{\mu}$ and immediately moves into the $\mu_{1,2} > 0$ quadrant (and thence through the upper boundary of Fig. 8). This accords with the theory of Section 3.2. An SWHe bifurcation curve emerges from $\mu = 0$, and an SWHo bifurcation curve emerges from $\mu = \tilde{\mu}$; we were not able to compute a complete locus of these bifurcation sets using AUTO, but indicate parts of them in Fig. 8. We also find an Sh bifurcation curve emerging from $\mu = \tilde{\mu}$, which almost coincides with one of the H bifurcation curves: see Fig. 8.

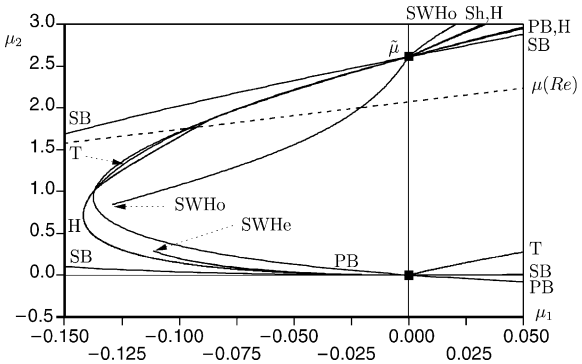

Fig. 8. Various bifurcation sets for (2) with $B_1 = 0.4375$, $B_2 = 1.2031$ and $\sigma_\mu = -1$ featuring symmetry-breaking (SB) pitchfork, Hopf (H), standing wave homoclinic (SWHo), standing wave heteroclinic (SWHe), Silnikov (Sh), parity-breaking (PB) and torus (T) bifurcations. The dashed line $\mu(Re)$ corresponds to changing the Reynolds number Re in a model in [3]; see (66).

For $\mu_2 \in (0, 1.0)$, the bifurcation sequence as μ_1 is increased from negative to positive values is very similar to that discussed in Section 4.1. We thus concentrate on $\mu_2 \in (1.0, 2.6122)$ and, in particular, the range in which the sequence is PB → T → H. The dashed curve in Fig. 8 provides a representative path through this region. As described in [14], it corresponds to monotonic increase of Reynolds number Re in the 0:1:2 three-mode reduction of plane Couette flow in a moderate aspect ratio domain [3]. The formula for this curve is given by

$$\begin{aligned} \mu_1(Re) &= \frac{(0.0323Re - 12.0680)}{11.4349}, \\ \mu_2(Re) &= \frac{(0.1062Re - 15.9763)}{11.4349}. \end{aligned} \tag{66}$$

In Fig. 9 we join the stable MM branch to the left of its encounter with PB at $Re \approx 339.53$, where it loses stability to TW solutions. A Hopf bifurcation subsequently occurs at $Re \approx 339.82$, producing SW solutions, and the MM equilibria converge on the origin at $Re \approx 373.61$ as the $\mu(Re)$ path in Fig. 8 crosses the $\mu_1 = 0$ axis. Meanwhile the TW solutions remain stable until $Re \approx 341$, where MTW solutions appear; these remain stable until $Re \approx 354.82$, at which point a PD bifurcation occurs. The resulting period-doubled MTW solutions enjoy a brief region of stability until $Re \approx 357.56$, where another PD bifurcation occurs (not shown in Fig. 8). The resulting period-doubled solutions lose stability at $Re \approx 357.93$; beyond this point all TW, MTW solutions and period-doubled variants are unstable. The unstable SW solutions arising in the H bifurcation at $Re \approx 339.82$ undergo T and PD bifurcations at $Re = 351.64$ and 352.59, respectively. Neither of the resulting (unstable) branches are shown in Fig. 8. The unstable SW solutions disappear altogether at $Re \approx 366.24$, when the SWHo line of Fig. 8 is crossed.

At the end of Section 3.1 we argued that structurally stable heteroclinic cycles of AGH type [2] must also occur for the 0:1:2 system (cf. Fig. 2); we now show projections of an example of this heteroclinic cycle, found at parameters (66) for $Re = 400$, in Fig. 10. (Note that the $x_1 = 0$ line is attracting despite the positive value of μ_1.) In addition to AGH cycles, there exist near $Re = 347$ (where $\mu_1 \approx -0.0752$ and $\mu_2 \approx 1.8257$) heteroclinic cycles of a type not previously seen. Their connecting orbits pass very close to the (unstable) MM_0 equilibrium in the real subspace (43) en route from the PM_0 equilibrium to the $PM_{\pi/2}$ equilibrium and then, during the return-path, close to $MM_{\pi/2}$: Fig. 11. An exact connection between the PM and MM fixed points is codimension two, since it requires coincidence of the one-dimensional unstable manifold of the PM solution with the one-dimensional stable manifold of the MM solution within the three-dimensional real subspace. There is no obvious reason why an approximate connection should occur for the cut through parameter space corresponding to the plane Couette flow model. However, such heteroclinic cycles cannot occur in the 1:2 system since the MM solutions would have an unstable complex conjugate

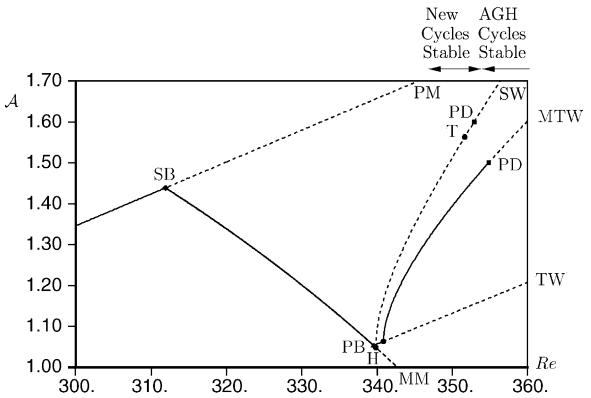

Fig. 9. Partial bifurcation diagram of (2) following the path $\mu(Re)$ given by (66) with system parameters (65). Here and on subsequent bifurcation diagrams for the 0:1:2 mode interaction, $\mathcal{A} = \sqrt{\max(|a_0|^2 + |a_1|^2 + |a_2|^2)}$.

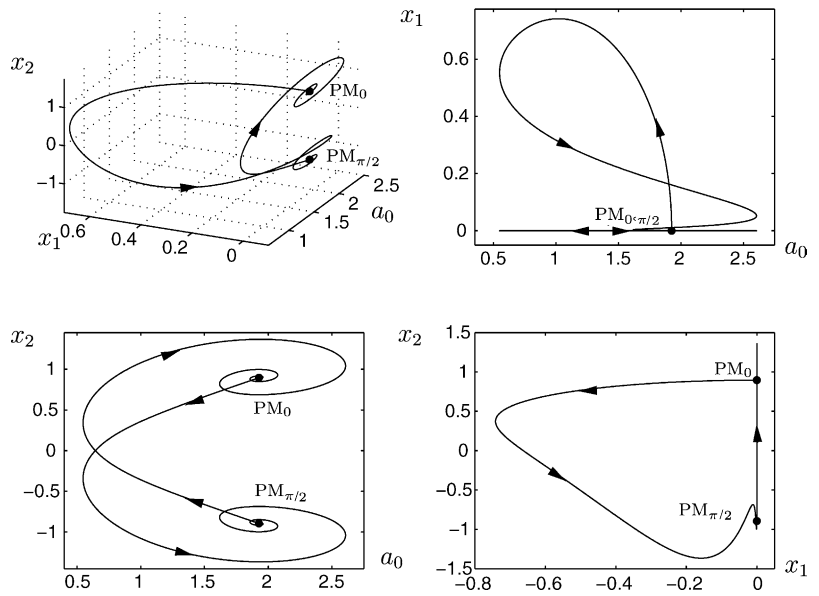

Fig. 10. Projections of the AGH type heteroclinic cycle $\mathrm{PM}_0 \to \mathrm{PM}_{\pi/2} \to \mathrm{PM}_0$ at $(\mu_1, \mu_2, B_1, B_2) = (0.0745, 2.318, 0.4375, 1.2031)$ (i.e. $Re = 400$). For these parameter values there are no MM equilibria to disrupt the cycle.

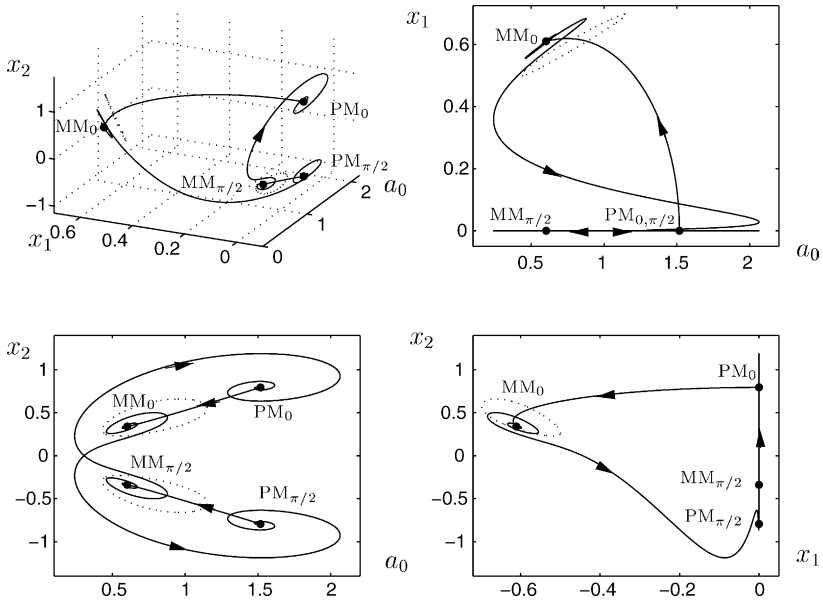

Fig. 11. Projections of the new heteroclinic cycle $\mathrm{PM}_0 \to \mathrm{MM}_0 \to \mathrm{PM}_{\pi/2} \to \mathrm{MM}_{\pi/2} \to \mathrm{PM}_0$ co-existing with a stable SW solution (dotted) at $(\mu_1, \mu_2, B_1, B_2) = (-0.0752, 1.8257, 0.4375, 1.2031)$ (i.e. $Re = 347$). This figure strongly suggests that the heteroclinic cycle (solid) passes *through* the two SW periodic orbits near MM_0 and $\mathrm{MM}_{\pi/2}$ (dotted) in the invariant real subspace.

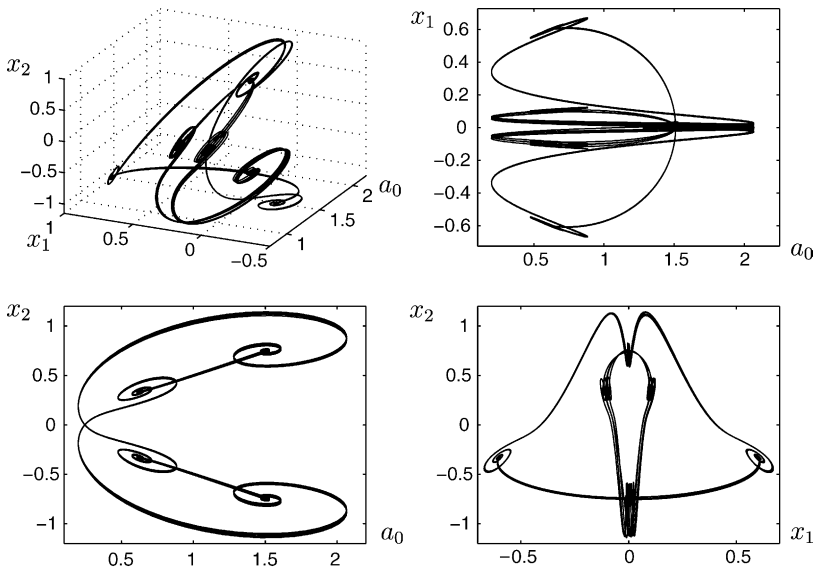

Fig. 12. Projections of the chaotic heteroclinic cycle $\mathrm{PM}_{\phi_1} \to \mathrm{MM}_{\phi_2} \to \mathrm{PM}_{\phi_3} \to \mathrm{MM}_{\phi_4} \to \mathrm{PM}_{\phi_5}$ at $(\mu_1, \mu_2, B_1, B_2) = (-0.0780, 1.8163, 0.4375, 1.2031)$ (i.e. $Re = 346$).

pair of eigenvalues in the two-dimensional real subspace (see Fig. 11), leaving no possible stable direction for a trajectory from a PM solution to come in along.

Fig. 11 also reveals that a stable heteroclinic connection can co-exist with stable SW solutions, shown as dotted loops near MM_0 and $\mathrm{MM}_{\pi/2}$. These SW orbits apparently nontrivially link the heteroclinic cycle in the (three-dimensional) real subspace.

For $Re = 346$, where $\mu_1 \approx -0.0780$ and $\mu_2 \approx 1.8163$, a cycle similar to that shown in Fig. 11 is found, but the visits to the MM equilibria are more complicated. Indeed, this appears to be a chaotic heteroclinic cycle; see Fig. 12. Here successive visits to MM solutions occur in a chaotic fashion, as shown in the left panel of Fig. 13, unlike the successive visits for $Re = 347$ which are always to one of four MM solutions related by $\pi/2$ rotations in the (x_1, y_1) plane, as shown in the right panel of Fig. 13.

We conclude this section by examining a horizontal path at $\mu_2 = 2.9$, intersecting the $\mu_1 = 0$ axis above $\mu = \tilde{\mu}$, the bifurcation diagram for which appears in Fig. 14. As deduced in Section 3.1, the MM equilibria in the right

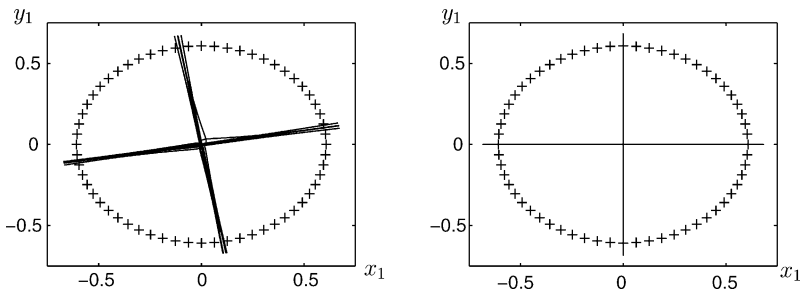

Fig. 13. Trajectory for solution shown in (left) Fig. 12 and (right) Fig. 11, with longer integration time. The +'s show the circle of MM fixed points. In the left panel, successive visits to MM solutions occur in a chaotic fashion. In the right panel, the successive visits are always to one of four MM solutions related by $\pi/2$ rotations in the (x_1, y_1) plane.

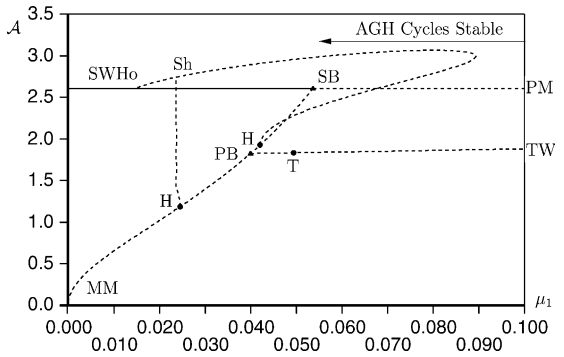

Fig. 14. Partial bifurcation diagram of (2) with system parameters (65) and $\mu_2 = 2.9$.

half-plane exist outside the parabola (45). These unstable MM equilibria bifurcate from the origin as μ_1 passes through zero and eventually disappear in a SB bifurcation at $\mu_1 = 0.0537$. Along the way, they undergo two H bifurcations at $\mu_1 = 0.0246$ and 0.0421. The SW solution emerging from the former bifurcation disappears in an apparent Sh bifurcation at $\mu_1 = 0.0236$, while the SW solutions emerging from the latter disappear in a SWHo bifurcation at $\mu_1 = 0.0144$. The two H bifurcations are separated by a PB bifurcation at $\mu_1 = 0.0400$, in which TW solutions are generated. These have four unstable eigenvalues, but two cross into the left half-plane at the T bifurcation at $\mu_1 = 0.0494$, and two more at the T bifurcation at $\mu_1 = 0.8800$ (not shown), giving stability of the TW solutions for higher μ_1 values. At the latter T bifurcation, the MTW solutions bifurcate to smaller values of μ_1, and are stable until undergoing their own T bifurcation at $\mu_1 = 0.4969$ (not shown). The MTW which emerge from the T bifurcation at $\mu_1 = 0.0494$ undergo various bifurcations, but always remain unstable.

5. Example 2: $B_1 = 0.5974$, $B_2 = -0.1149$, $\sigma_\mu = -1$

Our second example of the degenerate 1:2 and 0:1:2 resonances, representative of the case $\sigma_\mu = -1$ and $B_1 > 0$, $B_2 < 0$, is also taken from a low-dimensional plane Couette flow model, but in this case in a minimal flow unit [4]. Here dynamical structures such as travelling and standing waves that are present in a somewhat larger model (but which are similar to those considered in §3.1) account for the streak breakdown/reformation cycle in this flow. This parallels the discovery of structurally stable heteroclinic cycles in the five-mode boundary layer models in [8] and their subsequent elucidation in the simpler 1:2 resonance in [2].

5.1. Degenerate 1:2 resonance

We now study (26) for the particular case

$$e_{11} = -0.7138, \qquad e_{12} = e_{21} = 0.1373, \qquad e_{22} = -0.0264. \tag{67}$$

As in Section 4.1, we first find parabolae of SB and PB bifurcations. Since $\sigma_\mu = -1$ and $B_2 < 0$ the former is confined to the $\mu_2 \geq 0$ half-plane and (46) indicates that its extremum lies in the $\mu_{1,2} > 0$ quadrant; from (44) we see that the MM equilibria exist inside the parabola for $\mu_1 < 0$ and outside the parabola for $\mu_1 > 0$. The inequality $B_1 > -B_2/2$ is satisfied for this case and so (50) indicates that the locus of PB bifurcations has its extremum in the $\mu_1 < 0$, $\mu_2 > 0$ quadrant. Finally, since $\sigma_B = \text{sign}(B_1 B_2) < 0$, the line along which the MM equilibria are undefined *does* intersect the region in which these equilibria exist, as indicated by 'MM $\to \infty$' in Fig. 15.

We use AUTO to compute loci of H, T and SWHe bifurcations, all of which are indicated in Fig. 15. Again, in accord with the theory of Section 2.2, we see that the H bifurcation curve enters the $\mu_1 < 0$ half-plane and limits

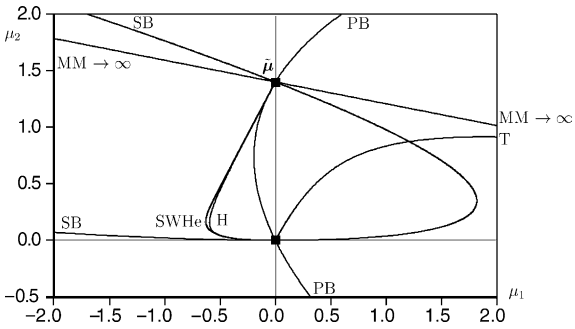

Fig. 15. Various bifurcation sets for (4) at with $e_{11} = -0.7138$, $e_{12} = e_{21} = 0.1373$ and $e_{22} = -0.0264$ featuring symmetry-breaking (SB) pitchfork, Hopf (H), standing wave heteroclinic (SWHe), parity-breaking (PB) and torus (T) bifurcations.

on $\tilde{\mu} = (0, -1/e_{11}) = (0, 1.400)$. The degenerate equilibria and some sample trajectories in parameter space are shown in Fig. 16; note the two branches of equilibria, since $\sigma_\mu \sigma_B > 0$. We find that the locus of SWHe bifurcations lies entirely *outside* that of the H bifurcations, while the locus of T bifurcations extends from the $\mu = 0$ point into the $\mu_1 > 0$ half-plane.

The situation here is clearly much simpler than in Section 4.1; as μ_1 increases from (moderate) negative to positive values for $\mu_2 \in (0, \tilde{\mu})$, the only bifurcation sequence observed is SWHe → H → PB → T → SB, possibly preceded by a further SB. A bifurcation diagram for $\mu_2 = 0.2$ is shown in Fig. 17. The MM equilibria, born in a SB bifurcation at $\mu_1 \approx -3.7945$, lose stability in a subcritical H bifurcation at $\mu_1 \approx -0.5909$. Between this and the SWHe bifurcation at $\mu_1 \approx -0.6234$ there exists an unstable SW solution, whose stable manifold divides the basins of attraction of the stable MM and $PM_{\pi/2}$ equilibria. Unstable TW solutions bifurcate from the unstable MM equilibria at $\mu_1 \approx -0.0880$, and later gain stability in a T bifurcation at $\mu_1 \approx 0.1202$, at which the stable MTW solutions disappear. Stable heteroclinic cycles of AGH type [2] exist in the region $\mu_1 \in (-0.61, -0.05)$; for the lowest values of μ_1 in this range the stable cycles co-exist with stable MM equilibria.

We close with a brief comment on the case $\mu_2 < 0$. Here the trivial state is the unique global attractor for $\mu_1 < 0$; moving into the $\mu_1 > 0$ half-plane, the mixed-mode equilibria bifurcate from $\mu = 0$ point and remain stable until bifurcating to travelling waves as the PB curve of Fig. 15 is crossed.

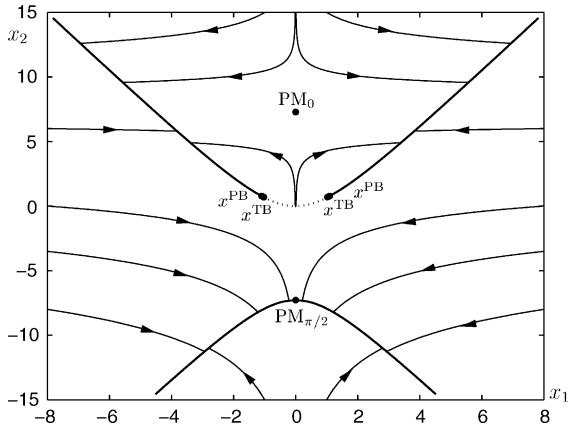

Fig. 16. Phase space of (26) for system parameters (67) at $\mu = \tilde{\mu}$ with sample trajectories. The nearly-coincident pure mode equilibria and Takens-Bogdanov points are labelled PM and TB, respectively. Compare this figure, for which $\sigma_\mu \sigma_B > 0$, with Fig. 5 where $\sigma_\mu \sigma_B < 0$.

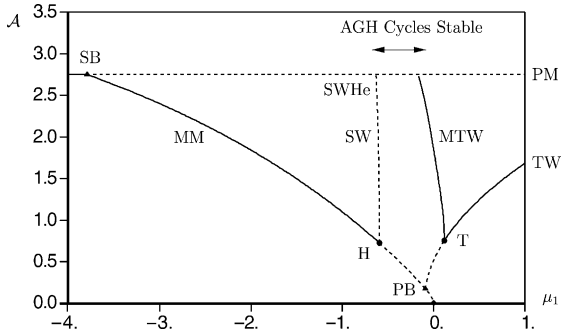

Fig. 17. Bifurcation diagram for (26) with parameters set according to (67) for fixed $\mu_2 = 0.2$.

5.2. 0:1:2 Resonance

We next turn to the full system (2) with system parameters (67), for which the curves of SB and PB bifurcations, as well as that along which the MM equilibria diverge to infinity, coincide with those found in Section 5.1.

We again turn to AUTO to numerically compute the locus of H, SWHe and T bifurcations departing from the $\mu = 0$ point, finding that the H bifurcation curve appears to diverge to infinity in the left half-plane and, in particular, does *not* pass through $\mu = \tilde{\mu}$, in accord with the theory of Section 3.2. The locus of SWHe bifurcations, computed with AUTO, are found to lie between the loci of SB and H bifurcations. The bifurcation sequence with fixed $\mu_2 \in (0, -1/e_{11})$ and μ_1 increasing through negative values to $\mu_1 = 0$ is thus expected to be the same as found in the degenerate 1:2 resonance. In the $\mu_1 > 0$ half-plane, however the picture differs somewhat from that of Section 5.1. Here it appears that most horizontal cuts through Fig. 18 do *not* intersect the T bifurcation locus (at least for moderate μ_1) and hence TW solutions appear to be the final limiting state.

For horizontal cuts with μ_2 set to a fixed value greater than $-1/e_{11}$, the branch of H bifurcations which depart the $\mu = \tilde{\mu}$ point is encountered, along with an associated SWHo bifurcation set.

We indicate by a dashed line in Fig. 18 the path followed through μ parameter space as the Reynolds number, Re, is monotonically increased in a 0:1:2 three-mode reduction of plane Couette flow in the minimal flow unit [4]. No interesting bifurcations are encountered as Re is increased from zero, the only qualitative change being the birth of MM solutions from the origin as the line crosses the $\mu_1 = 0$ axis (at $Re = 76.70$). The lack of interesting dynamics at these parameter values illustrates why the 0:1:2 mode interaction alone is an unsatisfactory model; however, the

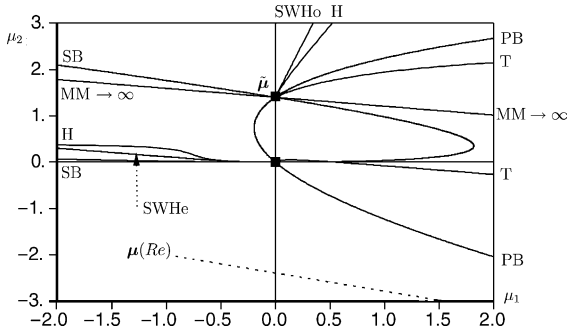

Fig. 18. Various bifurcation sets for (2) with $B_1 = 0.5974$, $B_2 = -0.1149$ and $\sigma_\mu = -1$ featuring symmetry-breaking (SB) pitchfork, Hopf (H), standing wave heteroclinic (SWHe), standing wave homoclinic (SWHo), parity-breaking (PB) and torus (T) bifurcations. The dashed line $\mu(Re)$ corresponds to changing the Reynolds number Re in the model obtained by restricting to the 0:1:2 modes in [4]. The equation for this line is $\mu_1(Re) = (0.1281Re - 9.8256)/10.7603$, $\mu_2(Re) = (-0.0503Re - 21.8841)/10.7603$.

addition of a few more modes to the basic 0:1:2 system leads to interesting, physically-relevant dynamical behavior similar to that of the 0:1:2 resonance at somewhat different parameter values [4].

6. Example 3: Perturbations from $\mu_{0,1,2} = 0$

At the outset of this paper, we rescaled (1) under the assumption of finite μ_0. We now discard this assumption, and consider the 0:1:2 resonance as a problem with three (small) bifurcation parameters μ_0, μ_1 and μ_2, allowing us to perturb from a (partially) integrable case. Throughout this section we restrict to the real subspace of (1) with c scaled out, and hence consider analogues of the first, second and fourth equations of (5) with μ_0 written for σ_μ (and $y_{1,2} = 0$). We focus on the case $B_1 > 0 > B_2$, for which an interesting family of periodic orbits are born in a 'Silnikov' homoclinic bifurcation [12].

For $\mu_j = 0$ the 'energy' function (3), which defines a family of ellipsoids in phase space, remains constant; for $\mu_j \neq 0$, we have

$$\dot{E} = \mu_0 a_0^2 + 2\mu_1 x_1^2 + 2\mu_2 x_2^2. \tag{68}$$

It will be convenient to define a new variable $\tilde{a}_0 \stackrel{\text{def}}{=} a_0/\sqrt{2}$ and system parameters $\tilde{B}_{1,2} \stackrel{\text{def}}{=} \sqrt{2}B_{1,2}$ so that the level sets of E become geometrical spheres $E = \tilde{a}_0^2 + x_1^2 + x_2^2$, and the (real) ODEs take the form

$$\begin{aligned} \dot{\tilde{a}}_0 &= \mu_0 \tilde{a}_0 + \tilde{B}_1 x_1^2 + \tilde{B}_2 x_2^2, \\ \dot{x}_1 &= (\mu_1 - \tilde{B}_1 \tilde{a}_0) x_1 + x_1 x_2, \\ \dot{x}_2 &= (\mu_2 - \tilde{B}_2 \tilde{a}_0) x_2 - x_1^2. \end{aligned} \tag{69}$$

For $\mu_j = 0$ the fixed points of (69) include two equilibria on the $\tilde{a}_0$ axis at

$$(\tilde{a}_0, x_1, x_2) = (\pm\sqrt{E}, 0, 0), \tag{70}$$

with eigenvalues

$$\lambda = 0, \mp\tilde{B}_1\sqrt{E} \text{ and } \mp\tilde{B}_2\sqrt{E}. \tag{71}$$

For $\tilde{B}_2 < 0 < \tilde{B}_1$, these are saddles; those with positive (resp., negative) $\tilde{a}_0$ having their stable eigenspaces in the x_1 (resp., x_2) direction and unstable eigenspaces in the x_2 (resp., x_1) direction. There are also four MM equilibria at the points

$$(\tilde{a}_0, x_1, x_2) = (\tilde{a}_0, \pm\sqrt{-\tilde{B}_1\tilde{B}_2}\tilde{a}_0, \tilde{B}_1\tilde{a}_0), \tag{72}$$

where

$$\tilde{a}_0 = \pm\sqrt{\frac{E}{1 + \tilde{B}_1(\tilde{B}_1 - \tilde{B}_2)}}; \tag{73}$$

the eigenvalues at these points are

$$\lambda = 0, \left(\frac{\tilde{a}_0\tilde{B}_2}{2}\right)\left(1 \pm \sqrt{1 + 8(\tilde{B}_1/\tilde{B}_2 + \tilde{B}_1^3/\tilde{B}_2 - \tilde{B}_1^2)}\right). \tag{74}$$

The radical in (74) may be positive for some choices of $\tilde{B}_1$ and $\tilde{B}_2$, but is negative for all $\tilde{B}_2 < 0$ provided $\tilde{B}_1 > 1/2\sqrt{2}$. Since $\tilde{B}_2$ is assumed negative, the real part of the nontrivial eigenvalues will share the sign of $\tilde{a}_0$. Thus, with $\tilde{B}_1 > 1/2\sqrt{2}$ Eq. (69) with $\mu_{0,1,2} = 0$ has two spiral sources in the $\tilde{a}_0 > 0$ half-space, and two spiral sinks in the $\tilde{a}_0 < 0$ half-space, on each invariant sphere.

In terms of the spherical polar coordinate representation

$$\tilde{a}_0 = r\,\cos\,\theta, \qquad x_1 = r\,\sin\,\theta\,\cos\,\varphi, \qquad x_2 = r\,\sin\,\theta\,\sin\,\varphi, \tag{75}$$

(where we restrict θ to $[0, \pi]$ and φ to $[0, 2\pi)$) (69) becomes

$$\begin{aligned}
\dot{r} &= (\mu_0\,\cos^2\,\theta + (\mu_1\,\cos^2\,\varphi + \mu_2\,\sin^2\,\varphi)\sin^2\,\theta)r,\\
\dot{\theta} &= \sin\,\theta[(\mu_1\,\cos^2\,\varphi + \mu_2\,\sin^2\,\varphi - \mu_0)\cos\,\theta - r(\tilde{B}_1\,\cos^2\,\varphi + \tilde{B}_2\,\sin^2\,\varphi)],\\
\dot{\varphi} &= (\mu_2 - \mu_1 + (\tilde{B}_1 - \tilde{B}_2)r\,\cos\,\theta)\sin\,\varphi\,\cos\,\varphi - r\,\sin\,\theta\,\cos\,\varphi.
\end{aligned} \tag{76}$$

As expected, setting $\mu_{0,1,2} = 0$ yields trivial radial dynamics $\dot{r} = 0$ and thus an invariant sphere $r = \sqrt{E}$, while the angular variables reveal that fixed points lie at $(\varphi, \theta) = (m\pi/2, n\pi)$ for any integers $m = 0, 1, 2, 3$ and $n = 0, 1$ and at (φ, θ) such that

$$\tan\,\varphi = \pm\sqrt{-\tilde{B}_1/\tilde{B}_2}, \qquad \tan\,\theta = \pm\sqrt{\tilde{B}_1(\tilde{B}_1 - \tilde{B}_2)}. \tag{77}$$

These latter conditions yield four equilibria, at

$$(\varphi, \theta) = (\bar{\varphi}, \bar{\theta}), \quad (\pi - \bar{\varphi}, \bar{\theta}), \quad (\pi + \bar{\varphi}, \pi - \bar{\theta}) \quad \text{and} \quad (2\pi - \bar{\varphi}, \pi - \bar{\theta}), \tag{78}$$

where

$$\bar{\varphi} = \arctan\sqrt{-\tilde{B}_1/\tilde{B}_2} \quad \text{and} \quad \bar{\theta} = \arctan\sqrt{\tilde{B}_1(\tilde{B}_1 - \tilde{B}_2)}. \tag{79}$$

For the system parameters $B_1 = 0.5974$, $B_2 = -0.1149$ of Section 5, $\bar{\varphi} \approx 1.1575$ and $\bar{\theta} \approx 0.9106$. The phase space of (76) for this case (at $r = 1$) is shown in Fig. 19. The fixed points (70) at the north and south poles are blown up to invariant circles at $\theta = 0, \pi$, and the four equilibria (78) appear as spiral sinks and sources above and below the equator $\theta = \pi/2$. Almost every initial condition is attracted to one of the sinks.

We now consider how this picture changes as the bifurcation parameters are perturbed away from zero. First, for the special case $\mu_{0,1,2} \equiv \mu$, the first equation of (76) decouples as $\dot{r} = \mu r$. In the $\tilde{a}_0, x_1, x_2$ coordinates, this implies a solution of (69) of the form

$$(\tilde{a}_0, x_1, x_2) = (\tilde{a}_0(0)\mathrm{e}^{\mu t}, \pm\sqrt{-\tilde{B}_1\tilde{B}_2}\,\tilde{a}_0(0)\mathrm{e}^{\mu t}, \tilde{B}_1\tilde{a}_0(0)\mathrm{e}^{\mu t}), \tag{80}$$

on the invariant radial lines $x_1 = \pm\sqrt{-\tilde{B}_1\tilde{B}_2}\,\tilde{a}_0$, $x_2 = \tilde{B}_1\,\tilde{a}_0$. Moreover, the terms involving μ_j in the second and third equations of (76) vanish identically, so that the θ, ϕ dynamics remain as in Fig. 19 while solutions move radially according to (80). No mixed modes exist in this case.

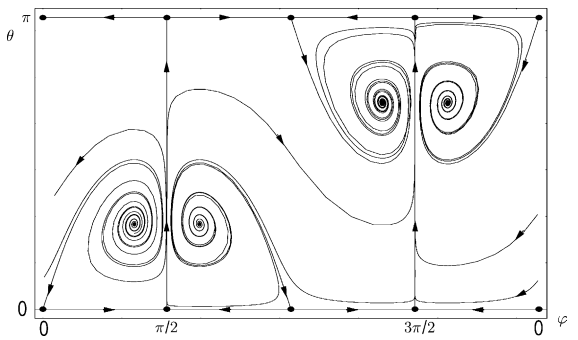

Fig. 19. Flow of the system (76) on $r = \text{const.}$ with $\mu_j = 0$.

For general $\mu_j \neq 0$ we may compute *approximate* invariant lines by substituting the ansatz

$$x_1 = \pm\sqrt{-\tilde{B}_1\tilde{B}_2}\,(\tilde{a}_0 + \alpha_1) \quad \text{and} \quad x_2 = \tilde{B}_1\,(\tilde{a}_0 + \alpha_2) \tag{81}$$

into (69) and equating coefficients of $\tilde{a}_0$ and $(\tilde{a}_0)^0$ (constant) (those of $\tilde{a}_0^2$ vanish identically, as above). This yields two pairs of equations:

$$\begin{aligned} &\mathcal{O}(\tilde{a}_0) : \mu_1 + \tilde{B}_1\alpha_2 = \mu_0 + 2\tilde{B}_1^2\tilde{B}_2(\alpha_2 - \alpha_1), \quad \mu_2 - \tilde{B}_2\alpha_2 + 2\tilde{B}_2\alpha_1 = \mu_0 + 2\tilde{B}_1^2\tilde{B}_2(\alpha_2 - \alpha_1);\\ &\mathcal{O}(1) : (\mu_1 + \tilde{B}_1\alpha_2)\alpha_1 = \tilde{B}_1^2\tilde{B}_2(\alpha_2^2 - \alpha_1^2) \quad \mu_2\alpha_2 + \tilde{B}_2\alpha_1^2 = \tilde{B}_1^2\tilde{B}_2(\alpha_2^2 - \alpha_1^2). \end{aligned} \tag{82}$$

These four equations can only be satisfied for the special choice $\mu_j \equiv \mu$ as above (whence $\alpha_j = 0$), but the first pair admits the solution

$$\begin{aligned} \alpha_1 &= \frac{(\mu_1 - \mu_2)(2\tilde{B}_1\tilde{B}_2 - 1)}{2\tilde{B}_2[\tilde{B}_1(\tilde{B}_2 - \tilde{B}_1) - 1]} + \frac{(\mu_1 - \mu_0)(\tilde{B}_1 + \tilde{B}_2)}{2\tilde{B}_2[\tilde{B}_1^2(\tilde{B}_2 - \tilde{B}_1) - \tilde{B}_1]},\\ \alpha_2 &= \frac{\mu_1 - \mu_0 + \tilde{B}_1^2(\mu_1 - \mu_2)}{\tilde{B}_1^2(\tilde{B}_2 - \tilde{B}_1) - \tilde{B}_1} \end{aligned} \tag{83}$$

for arbitrary μ_j. Choosing α_j thus, we balance the linear and quadratic terms, implying that, for large $|\tilde{a}_0|$, the affine linear subspaces (81) are increasingly good approximations to the distinguished solution curves of (76) that perturb from the lines (80) for $\mu_j \neq 0$.

The mixed modes (43) discussed in Section 3.1 may be written as

$$(\tilde{a}_0, x_1, x_2) = \left(\frac{\mu_1 B}{\mu_0 + \tilde{B}_1 B}, \frac{\pm\sqrt{-\mu_0\mu_1(\mu_0\mu_2 + B^2)}}{\mu_0 + \tilde{B}_1 B}, \frac{-\mu_0\mu_1}{\mu_0 + \tilde{B}_1 B}\right), \tag{84}$$

where $B = \mu_2\tilde{B}_1 - \mu_1\tilde{B}_2$. These fixed points exist only for $\mu_0\mu_1(\mu_0\mu_2 + B^2) < 0$ and they bifurcate from the pure modes $(\mu_2/\tilde{B}_2, 0, \pm\sqrt{-\mu_0\mu_2}/\tilde{B}_2)$, at

$$\mu_0 = -\frac{B^2}{\mu_2}, \tag{85}$$

which, under the redefinition $\mu_j \mapsto \mu_j/|\mu_0|$ employed above, coincides with (45). When $\mu_0 \to 0$ they collapse onto the (invariant) $\tilde{a}_0$-axis at $\tilde{a}_0 = \mu_1/\tilde{B}_1$, which is filled with fixed points at $\mu_0 = 0$. Similarly, the condition (47) at which the mixed modes reach infinity becomes

$$\mu_0 = -\tilde{B}_1 B. \tag{86}$$

As $\mu_0 \to -\tilde{B}_1 B$, the ratios $|x_1/\tilde{a}_0|$ and $|x_2/\tilde{a}_0|$ in (84) approach $\sqrt{-\tilde{B}_1\tilde{B}_2}$ and $\tilde{B}_1$ as required by the approximation (81).

It is easiest to describe the mixed modes as μ_0 varies for fixed μ_1, μ_2. There are several cases, depending on the signs of μ_1, μ_2 and B. We shall focus on those for $\mu_1 > 0 > \mu_2$ (with $\tilde{B}_2 < 0 < \tilde{B}_1$ as already noted). From (84)–(86), the mixed modes depart from the pure modes and move towards infinity with $\tilde{a}_0, x_2 > 0$ for $\mu_0 \in (-B^2/\mu_2, -\tilde{B}_1 B)$, and return from infinity with $\tilde{a}_0, x_2 < 0$ for $\mu_0 > -\tilde{B}_1 B$, and approach $(0, \pm\sqrt{-\mu_1\mu_2}, -\mu_1)$ as $|\mu_0| \to \infty$. Far from the origin, stability properties transverse to the (approximate) invariant lines (81) are determined by the dynamics on the invariant spheres for $\mu_j = 0$; hence, the mixed modes are unstable transverse to (81) approaching $\tilde{a}_0, x_2 = +\infty$, and stable transverse to (81) as they reappear from $\tilde{a}_0, x_2 = -\infty$. Along the invariant lines stability is determined by the sign of the (θ, ϕ)-dependent coefficient of the first (radial) equation of (76). Substituting the $\mathcal{O}(\tilde{a}_0)$ terms of (81) into the polar coordinate transformation (75), we find that this is dominated for large r by $\text{sign}(\mu_0 + \tilde{B}_1 B)$. We conclude that the MM equilibria are saddle points with two-dimensional unstable

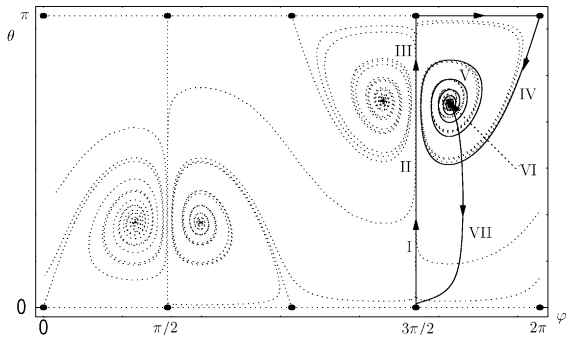

Fig. 20. Periodic orbit with bifurcation parameters $\mu_{0,1,2} = (0.01, 0.02, -0.02)$ and system parameters $B_1 = 0.5974$, $B_2 = -0.1149$, projected onto the (θ, ϕ) plane superimposed upon the trajectories of Fig. 19 (dotted). See the text for a discussion of phases I–VII.

and one-dimensional stable (two-dimensional stable and one-dimensional unstable) manifolds for $\mu_0 < -\tilde{B}_1 B$ ($\mu_0 > -\tilde{B}_1 B$), respectively.

For $\mu_0 > -\tilde{B}_1 B$ and sufficiently close to this value, the mixed mode saddle points are of 'dissipative' type, their positive real eigenvalues being smaller than the magnitude of the negative real parts of their complex conjugate pair. These fixed points are involved in a homoclinic bifurcation of Silnikov type [12], in which a family of remarkable periodic orbits is created. These were first found in numerical simulations, but they may be largely understood by reference to the behavior of solutions of (69) on the invariant plane $\mathcal{P} = \{(\tilde{a}_0, x_1, x_2) \mid x_1 = 0\}$, along the approximately-invariant lines and, for large $r = \sqrt{\tilde{a}_0^2 + x_1^2 + x_2^2}$, near the approximately-invariant spheres. The orbits display seven distinct phases, denoted I–VII, and an example is shown in Figs. 20 and 21. Due to reflection symmetry $x_1 \mapsto -x_1$ about $\mathcal{P}$, it suffices to consider only $x_1 \geq 0$.

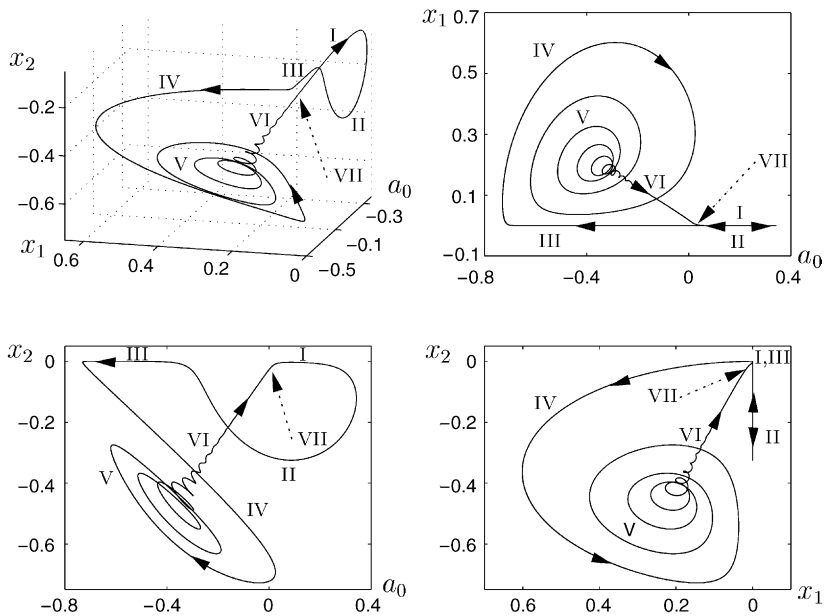

Fig. 21. Various projections of periodic orbit with $\mu_{0,1,2} = (0.01, 0.02, -0.02)$ and $B_1 = 0.5974$, $B_2 = -0.1149$.

First note that solutions starting near $\mathcal{P}$ remain near $\mathcal{P}$ for finite times, approaching it when the transverse dynamics governed by the second component of (69) is attractive, i.e. in the region $(\mu_1 - \tilde{B}_1\tilde{a}_0 + x_2) < 0$. The dynamics on $\mathcal{P}$ is topologically equivalent to that pictured in Fig. 1 *with time reversed*, since the signs of μ_0 (or σ_μ), μ_2 and $\tilde{B}_2$ in the present case are all opposite to the corresponding parameter signs in Fig. 1. Hence, all solutions starting sufficiently close to $\mathcal{P}$ (excepting those on stable manifolds of the mixed modes), eventually enter the half space $\tilde{a}_0 < 0$ and approach the negative $\tilde{a}_0$-axis. Here the quantity $(\mu_1 - \tilde{B}_1\tilde{a}_0 + x_2)$ becomes positive, and so $|x_1|$ begins to grow until the solution leaves the neighborhood of $\mathcal{P}$. This occurs explosively, since along the negative $\tilde{a}_0$-axis we have $\tilde{a}_0(t) = \tilde{a}_0(0)\exp(\mu_0 t)$, and using this in the linearized flow transverse to $\mathcal{P}$, we obtain

$$\dot{x}_1 = (\mu_1 - \tilde{B}_1\tilde{a}_0(t))x_1 \Rightarrow$$
$$x_1(t) = x_1(0)\exp\left[\mu_1 t - \frac{\tilde{B}_1\tilde{a}_0(0)}{\mu_0}(\exp(\mu_0 t) - 1)\right] \sim \exp\left[\mu_1 t - \frac{\tilde{B}_1\tilde{a}_0(0)}{\mu_0}\exp(\mu_0 t)\right], \tag{87}$$

and the second (superexponential) factor in the first exponent is positive for $\tilde{a}_0(0) < 0$. Flow near the positive $\tilde{a}_0$-axis, circulating with $|x_2|$ growing and shrinking, and along the negative $\tilde{a}_0$-axis forms phases I–III, and the superexponential explosion (87) initiates phase IV.

Once $|x_1|$ is $\mathcal{O}(1)$, x_2 grows again by virtue of the $-x_1^2$ term in the third equation of (69), all three components increase and the quadratic terms dominate, so that the orbit tracks the flow of the $\mu_j = 0$ system on an invariant sphere, spiraling towards one of the (stable) foci with $\tilde{a}_0, x_2 < 0$ in phase V: Fig. 20. It is now close to an attracting (approximate) invariant line, and will either escape to infinity or approach a neighborhood of $\mathcal{P}$ along that line, depending upon the flow direction at the point of initial approach. If the mixed mode saddle lies 'outside' this point, or lies in the region $\tilde{a}_0, x_2 > 0$, the dynamics returns the solution to $\mathcal{P}$ in phases VI and VII, the latter occuring close to $\mathcal{P}$ where linear terms dominate and $(\mu_1 - \tilde{B}_1\tilde{a}_0 + x_2) < 0$. This completes the periodic cycle; which however can be rather rich, since near $\mathcal{P}$ several circuits 'around' the pure mode $\mathrm{PM}_{\pi/2}$ may occur if the returning orbit lands near $\mathrm{PM}_{\pi/2}$ (the case of Figs. 20 and 21 has only a single circuit).

The above argument suggests only that there is an attracting set in the neighborhood of a closed curve that follows the route I–VII, but we may prove that this set exists, and that it is a stable periodic orbit, by appeal to a version of the Silnikov theorem appropriate to a dissipative spiral saddle for the eigenvalue conditions noted above ([15], p. 583, Fig. 4.8.26) and [16], cf. ([12], Theorem 6.5.1).

It remains then to verify that, for at least one parameter value $\mu_0 > 0$, the incoming branches of the unstable manifold(s) of the mixed mode(s) $\mathrm{MM}_{0,\pi/2}$, which follow the approximately-invariant lines (81) in towards $\mathcal{P}$, return to $\mathrm{MM}_{0,\pi/2}$. We first note that the flow on $\mathcal{P}$ (Fig. 1 with time reversed) implies that only solutions lying in the stable manifolds of the pure modes can limit on $\mathcal{P}$ (for $\mu_1 > 0$ the stable manifold of the origin lies in $\mathcal{P}$). Thus, while codimension two heteroclinic bifurcations *may* occur in which $W^{\mathrm{u}}(\mathrm{MM}_{0,\pi/2})$ limit on PM_0 or $\mathrm{PM}_{\pi/2}$, as one varies μ_0 with all other parameters fixed these will generically not be encountered.

We next observe that, as μ_0 increases in the range $(-\tilde{B}_1 B, \infty)$, $\mathrm{MM}_{0,\pi/2}$ move monotonically inward along the lines, carrying their (local) stable manifolds $W^{\mathrm{s}}(\mathrm{MM}_{0,\pi/2})$ with them. At large $|r|$, $W^{\mathrm{s}}(\mathrm{MM}_{0,\pi/2})$ remains close to the invariant spheres; consequently solutions departing from $\mathcal{P}$ in any bounded neighborhood of the origin, including solutions in $W^{\mathrm{u}}(\mathrm{MM}_{0,\pi/2})$, lie 'inside' $W^{\mathrm{s}}(\mathrm{MM}_{0,\pi/2})$ for μ_0 larger than, but sufficiently close to $-\tilde{B}_1 B$.

In contrast, we will show that the estimate (87) implies that, as μ_0 increases, the point on the negative $\tilde{a}_0$-axis at which $W^{\mathrm{u}}(\mathrm{MM}_{0,\pi/2})$ explodes away from $\mathcal{P}$ moves monotonically out towards $\tilde{a}_0 = -\infty$. Indeed, eliminating t from the linearized x_1 and $\tilde{a}_0$ equations of (69) and writing the initial values of x_1 and a_0 as x_{10} and a_{00}, respectively, we have:

$$\frac{\mathrm{d}x_1}{\mathrm{d}\tilde{a}_0} = \frac{\mu_1 x_1}{\mu_0\tilde{a}_0} - \frac{\tilde{B}_1 x_1}{\mu_0} \Rightarrow |x_1| = |x_{10}|\left|\frac{\tilde{a}_0}{\tilde{a}_{00}}\right|^{\frac{\mu_1}{\mu_0}}\exp\left[-\frac{\tilde{B}_1}{\mu_0}(\tilde{a}_0 - \tilde{a}_{00})\right]. \tag{88}$$

For $\mu_1, \tilde{B}_1 > 0$ and $(\tilde{a}_0 - \tilde{a}_{00}) < 0$ fixed, both the second and third factors in this expression decrease as $\mu_0\,(> 0)$ increases, so if we can show that $|x_{10}|$, the distance from $\mathcal{P}$ at which $W^{\mathrm{u}}(\mathrm{MM}_{0,\pi/2})$ first becomes close to the negative

$\tilde{a}_0$-axis, also decreases as μ_0 increases, our claim will follow. The points of first encounter of $W^{\mathrm{u}}(\mathrm{MM}_{0,\pi/2})$ with $\mathcal{P}$ may be estimated from (81) by setting $x_1 = 0$ to obtain $\tilde{a}_0 \approx -\alpha_1$, $x_2 \approx \tilde{B}_1(\alpha_2 - \alpha_1)$, with α_j given in (83):

$$(\tilde{a}_0, x_2) \approx \left(\frac{\mu_0(\tilde{B}_1 + \tilde{B}_2)}{2\tilde{B}_2[\tilde{B}_1^2(\tilde{B}_2 - \tilde{B}_1) - \tilde{B}_1]} + \text{const.}, \frac{\mu_0(\tilde{B}_1 - \tilde{B}_2)}{2\tilde{B}_2[\tilde{B}_1(\tilde{B}_2 - \tilde{B}_1) - 1]} + \text{const.} \right), \tag{89}$$

where the constant terms depend upon μ_1, μ_2, $\tilde{B}_1$, $\tilde{B}_2$ but are independent of μ_0. This implies that, as μ_0 increases, the approximate 'landing points' in $x_2 < 0$ move along a line

$$x_2 = \frac{\tilde{B}_1(\tilde{B}_1 - \tilde{B}_2)}{(\tilde{B}_1 + \tilde{B}_2)}\tilde{a}_0 + \mathcal{O}(\mu_0^{-1}), \tag{90}$$

thus approaching the $\tilde{a}_0$-axis, and the increase in μ_0 contributes to take solutions further from the origin as they track the circles in which the invariant sphere intersects $\mathcal{P}$. The time spent in phases I and II where $(\mu_1 - \tilde{B}_1\tilde{a}_0 + x_2) < 0$ and $\mathcal{P}$ is attractive is therefore increased, effectively reducing the value of $|x_{10}|$ appropriate for the estimate (88). Consequently, for sufficiently large $\mu_0 > -\tilde{B}_1 B$, $W^{\mathrm{u}}(\mathrm{MM}_{0,\pi/2})$ leaves $\mathcal{P}$ 'outside' $W^{\mathrm{s}}(\mathrm{MM}_{0,\pi/2})$.

It follows from continuous dependence of solutions on parameters that there is at least one μ_0 for which attracting homoclinic cycles to $\mathrm{MM}_{0,\pi/2}$ exist, and the (modified) Silnikov result implies that there exist stable periodic orbits near this value. For example, for $\mu_1 = 0.02$, $\mu_2 = -0.02$, $B_1 = 0.5974$, and $B_2 = -0.1149$ (as considered in Section 5) such that $-\tilde{B}_1 B = 0.01153$, the homoclinic orbit occurs at $\mu_0 \approx 0.01181$. Here the eigenvalues of the MM are 0.000156 and $-0.08332 \pm 0.73736\mathrm{i}$. The unique stable periodic orbit associated with this homoclinic orbit can be followed to lower values of μ_0, as in Fig. 21.

While we appeal to the $\mu_{0,1,2} \to 0$ limit in accounting for the behavior of these periodic orbits in terms of solutions on invariant spheres, the parameter-rescaling symmetry $(a_j, \mu_j, t) \mapsto (\alpha a_j, \alpha\mu_j, t/\alpha)$ noted in Section 1 implies that any solution found (perturbatively) for small μ_j has an 'expanded' counterpart for large μ_j. Hence these orbits (and, indeed, all others) exist in an unbounded sector of parameter space. We note that these periodic orbits, which lie in the real subspace, appear to be stable and attracting for general initial conditions in the full 5-dimensional phase space: all solutions appear to eventually relax on a rotation of the real subspace, and approach one of the pair of periodic orbits therein. Analogous periodic orbits are not possible for the related 1:2 system, since they clearly require the a_0 direction (see Fig. 21).

7. Conclusions

In this paper we studied a five- (real) dimensional quadratic system originally derived though projection of the Navier-Stokes equations onto a subspace of three Fourier modes of wavenumbers 0, 1 and 2 [3,4], but relevant to more general three-wave interactions in systems with O(2) symmetry. In addition to this symmetry, the equations have a rather special structure: their homogeneous quadratic terms preserve an energy-like function, and they exhibit a scaling 'parameter symmetry.' Two limits are notable: when the three bifurcation parameters vanish, the conservative system preserves a family of invariant spheres, and when two of the parameters (μ_1, μ_2) are small relative to the third (μ_0), the (fast) 0-mode equation may be removed and the system collapsed to a degenerate case of the 1:2 resonance studied in [2] and [11].

We re-examined the 1:2 resonance and shed some light on the previously unstudied degenerate case. In addition to all the solution types described in [1,2,11], we found a parameter value $(\tilde{\mu})$ at which loci of symmetry-breaking, parity-breaking and Hopf bifurcations pass through the $\mu_1 = 0$ axis. This organizing center corresponds to a degenerate Takens-Bogdanov bifurcation point contained in either a closed curve, or two open arcs, of equilibria, depending upon the signs of the system parameters.

We used the 1:2 analysis as a stepping stone to the problem of the 0:1:2 three-wave resonance. Most notably, this system possesses analogues of the structurally stable heteroclinic cycles of [2] connecting pure modes, as well as

new cycles involving transits among both pure and mixed modes. We then considered the 1:2 and 0:1:2 resonance problems for two particular cases of system parameters typifying these new behaviors. We found significant differences between the 1:2 and 0:1:2 systems for the same parameter values, and were able to explain some of these differences. For example, the presence or absence of an additional locus of Hopf bifurcations emanating from $\tilde{\mu}$ in the 0:1:2 case depends only on the system parameter values (Fig. 3, Eqs. (63) and (64)). We also found a class of 'strange' periodic orbits that exist over a relatively large bifurcation and system parameter region, whose existence we prove by appeal to Silnikov bifurcation theory, and whose structure we interpret via the conservative limit.

While we have studied only the quadratic system (1) here, we expect that many of the phenomena described will persist locally, near $a_j = 0$ *for sufficiently small* $|\mu_j|$, for O(2)-equivariant systems with cubic and higher order terms that continue to preserve an 'energy like' integral analogous to (3). Of course, the parameter-rescaling symmetry $(a_j, \mu_j, t) \mapsto (\alpha a_j, \alpha\mu_j, t/\alpha)$ will no longer hold, but hyperbolic sets and codimension one and two bifurcations will continue to occur [12].

Acknowledgements

This work was supported by DoE: DE-FG02-95ER25238 (T.R.S. and P.J.H.) and a National Science Foundation Mathematical Sciences Postdoctoral Research Fellowship to J.M. We thank the referees for their careful reading and constructive comments.

References

[1] G. Dangelmayr, Steady-state mode interactions in the presence of O(2)-symmetry, Dyn. Stab. Syst. 1 (2) (1986) 159–185.
[2] D. Armbruster, J. Guckenheimer, P. Holmes, Heteroclinic cycles and modulated traveling waves in systems with O(2) symmetry, Physica D 29 (1988) 257–282.
[3] J. Moehlis, T.R. Smith, P. Holmes, H. Faisst, Models for turbulent plane Couette flow using the proper orthogonal decomposition, Phys. Fluids 14 (7) (2002) 2493–2507.
[4] T.R. Smith, J. Moehlis, P. Holmes, Low-dimensional models for turbulent plane Couette flow in a minimal flow unit, J. Fluid Mech. 538 (2005) 71–110.
[5] C. Nore, L.S. Tuckerman, O. Daube, S. Xin, The 1:2 mode interaction in exactly counter-rotating von Kármán swirling flow, J. Fluid. Mech 477 (2003) 51–88.
[6] C. Jones, M. Proctor, Strong spatial resonance and travelling waves in Bénard convection, Phys. Lett. A 121 (1987) 224–227.
[7] M. Proctor, C. Jones, The interaction of two spatially resonant patterns in thermal convection 1: exact 1:2 resonance, J. Fluid Mech. 188 (1988) 301–335.
[8] N. Aubry, P. Holmes, J.L. Lumley, E. Stone, The dynamics of coherent structures in the wall region of the turbulent boundary layer, J. Fluid Mech. 192 (1988) 115–173.
[9] I. Mercader, J. Prat, E. Knobloch, Robust heteroclinic cycles in two-dimensional Rayleigh-Bénard convection without Boussinesq symmetry, Int. J. Bifurcation Chaos 12 (11) (2002) 2501–2522.
[10] P. Holmes, J.L. Lumley, G. Berkooz, Turbulence, Coherent Structures, Dynamical Systems and Symmetry, Cambridge University Press, Cambridge, UK, 1996.
[11] J. Porter, E. Knobloch, New type of complex dynamics in the 1:2 resonance, Physica D 159 (2001) 125–154.
[12] J. Guckenheimer, P. Holmes, Nonlinear Oscillations, Dynamical Systems and Bifurcations of Vector Fields, Springer-Verlag, New York, NY, 1983.
[13] E. Doedel, A. Champneys, T. Fairgrieve, Y. Kuznetsov, B. Sandstede, X. Wang, AUTO 97: Continuation and bifurcation software for ordinary differential equations, Available via FTP from directory/pub/doedel/autoatftp.cs.concordia.ca, 1997.
[14] T. R. Smith, Low-dimensional Models of Plane Couette Flow using the Proper Orthogonal Decomposition, Princeton University, 2003.
[15] S.R. Wiggins, Introduction to Applied Nonlinear Dynamical Systems and Chaos, Springer-Verlag, New York, 1990.
[16] P. Glendinning, C. Sparrow, Local and global behavior near homoclinic orbits, J. Stat. Phys. 35 (1984) 645–696.